ISA Transactions 133 (2023) 397–411

Contents lists available at ScienceDirect

ISA Transactions

journal homepage: www.elsevier.com/locate/isatrans

Practice article

On the equivalence between Generalized Proportional Integral Observer and Disturbance Observer

Harvey David Rojas *, John Cortés-Romero

Department of Electrical and Electronic Engineering, Universidad Nacional de Colombia, Av. Cra. 30 # 45-03, Bogotá, Colombia

ARTICLE INFO

Article history:
Received 31 May 2021
Received in revised form 23 June 2022
Accepted 24 June 2022
Available online 28 June 2022

Keywords:
Active disturbance rejection control (ADRC)
Disturbance observer (DOB)
Extended state observer (ESO)
Generalized proportional integral observer (GPIO)
Robustness and performance analysis

ABSTRACT

This paper presents the equivalence between generalized proportional integral observer (GPIO) and disturbance observer (DOB), which is applicable to reduced-order GPIO (ROGPIO), full-order GPIO (FOGPIO), and extended state observer (ESO). From this equivalence, established in frequency-domain, comprehensive analyses are performed regarding the influence of the system order, the number of extended states, the uncertain control gain, and the tuning method on the robustness and performance of GPIO. In addition, the equivalence allows a detailed comparison between ROGPIO and FOGPIO in the active disturbance rejection control (ADRC) framework. Finally, experimental validation of the main results is presented for the study case of a synchronous buck converter.

1. Introduction

Disturbance rejection based control has become one of the most popular approaches for robust control due to its effectiveness, flexibility, and simplicity [1]. This control approach has been enriched from several research perspectives, whose common paradigm is the estimation and rejection of disturbances affecting the system. In general, disturbance estimation could include the identification of uncertainties, unmodeled dynamics, and external disturbances [2]. In this sense, an effective disturbance rejection allows accomplishing closed-loop specifications using classical control techniques [3].

In the context of disturbance estimation, extended state observer (ESO), generalized proportional integral observer (GPIO), and disturbance observer (DOB) are some of the most used methods. Their applications have been widely investigated and tested in different areas [3–5]. Classical DOB-based control (DOBC) uses a frequency-domain formulation not only for controller design but also for robustness analysis [6,7]. Furthermore, some DOB features, such as intuitive conceptualization and easy implementation, have been recognized by practitioners. On the other hand, ESO and GPIO are mainly presented in time-domain, and they are the core of active disturbance rejection control (ADRC). From ADRC perspective, both exogenous and endogenous disturbances are lumped into a total disturbance, which is represented as an extended state into the system model [2]. Then, by estimating and canceling the total disturbance, it is possible to force the plant to act as a desired reference model [8,9], which often takes an integrator chain form [10].

Given the rigorous stability analysis that the frequency-domain approach provides to DOBC, its equivalence with other control strategies has been explored, as shown in Table 1. It was reported in [11] that the passivity-based control (PBC) is a subset of DOBC and additional elements for the stability and performance analysis of DOB were revealed. The equivalence between unknown input disturbance observer, disturbance estimating filter, and PBC was presented in [12]. This study also provided some parameter selection rules for PBC. In order to find the equivalence between DOBC, internal model control (IMC), and a robust adaptive controller, a unified disturbance attenuation framework was proposed in [13]. In [14], a tuning method for Proportional Integral Derivative (PID) controllers was obtained from its equivalence with a DOB-aided PD controller. It was demonstrated in [15] that a combination of the state-space PI controller and a reduced-order observer becomes equivalent to DOBC in the context of discrete-time control for grid converters. Equivalence relations between a time-delayed controller (TDC) and a nonlinear DOBC under the nonmodel-based control framework of robot manipulators were analyzed in [16]. In addition, disturbance observer designs in the H_∞ control framework were presented in [17] and [18].

Regarding ADRC, [19] introduced the equivalence among PID controllers, flat filters (FF), control based on reduced-order ESO (RESO), and sliding mode control (SMC) for second-order plants. Similarly, in the context of integrator chain systems, the equivalence between ADRC with reduced-order GPIO (ROGPIO) and

* Corresponding author.
E-mail addresses: hdrojasc@unal.edu.co (H.D. Rojas), jacortesr@unal.edu.co (J. Cortés-Romero).

https://doi.org/10.1016/j.isatra.2022.06.032
0019-0578/

Table 1
Overview of studies on the equivalence between DOBC and other structures.

Equivalent structures		Approach	Nominal model	Main results	Ref.
DOBC	Passivity-based control (PBC)	Time-domain	*n*th order linear	Demonstration. Stability analysis of DOB.	[11]
Unknown input DOB	Disturbance estimating filter and PBC	Frequency-domain	*n*th order linear	Demonstration. Parameter selection rules for PBC	[12]
DOBC	Robust adaptive controller and IMC	Frequency-domain	*n*th order linear	Demonstration. Unified analysis-design framework	[13]
PD + DOB	PID	Frequency-domain	Second-order linear	Demonstration. Tuning rules for PID	[14]
DOBC	State-Space PI + reduced-order observer	Frequency-domain	Linear discrete (specific case)	Demonstration	[15]
DOBC	Time-delayed control	Time-domain	Nonmodel-based control of robots	Demonstration	[16]

Table 2
Overview of studies on the equivalence between ADRC and other structures.

Equivalent structures		Approach	Nominal model	Main results	Ref.
ADRC (RESO)	Flat filters, PID, and SMC	Frequency-domain	Second-order integrator chain. Applicable to *n*th order, except for PID	Demonstration	[19]
ADRC (ROGPIO)	Flat filters	Frequency-domain	*n*th order integrator chain	Demonstration	[10]
ADRC (RESO)	Flat filters	Frequency-domain	*n*th order integrator chain	Demonstration. Implementation of ADRC via Flat filters	[20]
ADRC (ESO)	PID + Low-pass filter	Frequency-domain	Second-order integrator chain	Demonstration	[21]
ADRC (ESO/RESO)	2-DOF PID and 2-DOF IMC	Frequency-domain	Second-order linear. Applicable to *n*th order	Demonstration. Implementation of ADRC via 2-DoF PID. Tuning rules for PID	[22]
P+ESO, P+RESO, PI+RPIO	Generalized PI controller	Frequency-domain	Second-order integrator chain	Demonstration. Generalized analysis framework	[23]
ADRC (RESO/ESO)	Linear finite-dimensional controller	Time-domain	*n*th order linear	Demonstration. Implementation of linear controllers via ADRC	[24]

FF was established in [10]. This equivalence was complemented in [20] through a frequency-domain analysis and experimental results, which revealed that RESO-based ADRC can be synthesized as a linear controller. In [21], ESO-based ADRC was interpreted as a PID compensator with a second-order low-pass filter. It was shown in [22] that RESO-based ADRC is equivalent to both two-degree-of-freedom (2-DoF) IMC and 2-DoF PID controller. This equivalence also provided tuning rules for PID, which facilitate the implementation of ADRC in industry. In [23], Proportional controller with ESO and RESO, and PI controller with reduced-order PI observer (RPIO) were analyzed in the context of second-order systems with an integrator chain form. This work showed that those three structures can be described as a type of generalized PI controller. The implementation of linear finite-dimensional controllers via ADRC was described in [24]. The aforementioned contributions are summarized in Table 2.

Several methods of improving the performance of ESO-based control, which consider the observer structure, tuning strategy, and working conditions, were studied in reviews [25,26]. Moreover, different issues in practical implementation of ADRC and the ways to face them were summarized in [27]. Although the time-domain performance of ESO-based ADRC has been largely discussed, its behavior in frequency-domain have been less explored [28]. Basic frequency response analyses concerning linear ESO were presented in [29–32]. A study based on the small gain theorem was proposed in [33], and some connections between frequency and time domain formulations were described in [9, 28]. As regards nonlinear ESO, the describing function method [34], the extended circle criterion [35], and the Popov criterion [36,37] have been the most used techniques for stability analysis.

Despite previous works have pointed out connections between ADRC and DOBC [1,3], the conditions for their equivalence have not been formally presented. Moreover, research about the relation between GPIO and DOB is even more scarce. Accordingly, this work presents the equivalence between GPIO and DOB with a frequency-domain approach. This equivalence is applicable to full-order GPIO (FOGPIO), reduced-order GPIO (ROGPIO), ESO, and RESO. thus facilitating a detailed comparison between them in the ADRC framework.

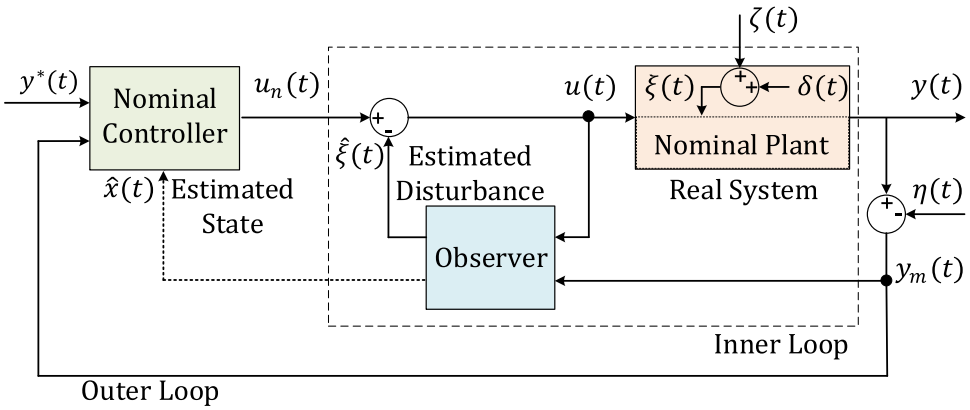

Fig. 1. Disturbance rejection based control.

The proposed equivalence allows a comprehensive analysis to identify the influence of the system order, the number of extended states, the uncertain control gain, and the tuning method on the robustness and performance of GPIO. As a result, some guidelines for its practical implementation are provided. In addition, the analysis motivated by this equivalence articulates several practical control requirements, such as accuracy, stability margins, and noise sensitivity. This articulation is a current need among researchers in the field of ADRC.

The remaining of this paper is organized as follows: Section 2 presents the equivalence between GPIO and DOB. Section 3 focuses on the robustness and performance analysis of GPIO. Section 4 describes a comparison between ROGPIO and FOGPIO in the ADRC framework. Section 5 shows an experimental validation of the main results on the voltage control of a synchronous buck converter. Finally, Section 6 summarizes the conclusions of this work.

2. Equivalence between GPIO and DOB

This section presents the equivalence between generalized proportional integral observer (GPIO) and disturbance observer (DOB). Firstly, the control based on disturbance estimation is introduced. Secondly, full-order GPIO (FOGPIO), reduced-order GPIO (ROGPIO), and DOB are deduced in time-domain. Subsequently, the equivalence between them is established with a frequency-domain approach. Finally, this equivalence is applied to full-order and reduced-order extended state observers.

2.1. Disturbance rejection based control

A general block diagram of the disturbance rejection based control is presented in Fig. 1. The dynamic system to be controlled has an input $u(t)$ and an output $y(t)$, whose measurement $y_m(t)$ is affected by noise $\eta(t)$. Consequently, it is required to find a control law $u(t)$ such that $y(t)$ tracks the reference trajectory $y^*(t)$. This goal must be achieved even in the presence of external disturbances $\zeta(t)$ and internal disturbances $\delta(t)$ caused by system uncertainties and unmodeled dynamics.

The control strategy is composed of two stages. Firstly, an inner loop uses an observer to estimate the total disturbance $\xi(t)$ that lumps $\delta(t)$ and $\zeta(t)$. In doing so, it is possible to reject $\xi(t)$ and impose a selected nominal model. Secondly, in the outer loop a feedback controller allows trajectory tracking through the control signal $u_n(t)$. This controller is designed for the nominal model, and it can use the estimate of the system state $\hat{\boldsymbol{x}}(t)$, if the observer supplies it. Finally, the plant input $u(t)$ combines the nominal control $u_n(t)$, and the estimated disturbance $\hat{\xi}(t)$.

The real plant in Fig. 1 can be a nonlinear system with a complex dynamic model. Nevertheless, since the objective of the inner loop is to enforce a certain reference model, it can have a linear structure. In this context, an integrator chain form significantly reduces the modeling requirements, and it is useful to deal with uncertain systems [2]. Therefore, consider a nonlinear system described by the following state-space model:

$$\begin{cases} \dot{\boldsymbol{x}}_p(t) = & \boldsymbol{A}_p\boldsymbol{x}_p(t) + \boldsymbol{B}_p\left(\kappa(\boldsymbol{x}_p,t)u(t) + \phi(\boldsymbol{x}_p,t) + \zeta(t)\right), \\ y(t) = & \boldsymbol{C}_p\boldsymbol{x}_p(t), \end{cases} \tag{1}$$

where $\boldsymbol{x}_p \triangleq [x_1 \dots x_n]^\top \in \mathbb{R}^n$ is the state vector, n is the system order, $u \in \mathbb{R}$ is the control signal, $y \in \mathbb{R}$ is the output, $\zeta \in \mathbb{R}$ is an external disturbance, $\kappa(\boldsymbol{x},t) \in \mathbb{R} \setminus \{0\}$ represents the influence of the control action on the system dynamics, $\phi \in \mathbb{R}$ is the remainder dynamics of the plant, $\boldsymbol{A}_p \triangleq \begin{bmatrix} \boldsymbol{0}^{(n-1)\times 1} & \boldsymbol{I}^{(n-1)\times(n-1)} \\ 0 & \boldsymbol{0}^{1\times(n-1)} \end{bmatrix} \in \mathbb{R}^{n\times n}$, $\boldsymbol{B}_p \triangleq \begin{bmatrix} \boldsymbol{0}^{1\times(n-1)} & 1 \end{bmatrix}^\top \in \mathbb{R}^n$, and $\boldsymbol{C}_p \triangleq \begin{bmatrix} 1 & \boldsymbol{0}^{1\times(n-1)} \end{bmatrix} \in \mathbb{R}^n$.

System dynamics (1) can be rewritten as follows:

$$\begin{cases} \dot{\boldsymbol{x}}_p(t) = & \boldsymbol{A}_p\boldsymbol{x}_p(t) + \boldsymbol{B}_p\kappa_n u(t) + \boldsymbol{B}_p\xi(t), \\ y(t) = & \boldsymbol{C}_p\boldsymbol{x}(t), \end{cases} \tag{2}$$

where κ_n is a nonzero constant that represents the nominal control gain and $\xi(t) = \kappa(\boldsymbol{x_p},t)u(t) - \kappa_n u(t) + \phi(\boldsymbol{x}_p,t) + \zeta(t)$ is the total disturbance.

Remark 1. Signal $\xi(t)$ in model (2) lumps external and state-dependent disturbances, which can include nonlinear terms [2]. Nevertheless, the total disturbance is assumed to be unknown, smooth, and uniformly absolutely bounded [19]. Under these conditions, $\xi(t)$ is also exponentially integrable, therefore, its Laplace transform denoted by $\Xi(s)$ is assumed to exist [20].

Next, different observers are designed to estimate the total disturbance and the equivalence between them is established.

2.2. Full-order GPIO

The total disturbance affecting system (2) can be locally approximated by a polynomial of degree $m-1$, whose coefficients are time-varying. This implies an ideal internal model of $\xi(t)$ such that $d^m\xi(t)/dt^m = 0$, for $t \geq 0$. Assuming that there exist a constant ϵ_m that satisfies the condition $\sup_t |\xi^{(m)}(t)| \leq \epsilon_m$, then, it is possible to obtain an online estimation of the total disturbance $\hat{\xi}(t)$, by means of an asymptotic observer with a bounded estimation error [5].

Now, let us define the extended state $\boldsymbol{x} \triangleq [x_1 \dots x_{n+m}]^\top \in \mathbb{R}^{n+m}$, which includes the system states $[x_1 \dots x_n]^\top$, and the augmented states $[x_{n+1} \dots x_{n+m}]^\top \triangleq [\xi \dots \xi^{(m-1)}]^\top$.

The dynamics of the extended state is expressed as

$$\begin{cases}\dot{\boldsymbol{x}}(t) = \boldsymbol{A}\boldsymbol{x}(t) + \boldsymbol{B}\kappa_n u(t) + \boldsymbol{H}\xi^{(m)}(t)\\ y(t) = \boldsymbol{C}\boldsymbol{x}(t)\end{cases} \tag{3}$$

where $\boldsymbol{A} \triangleq \begin{bmatrix}\boldsymbol{0}^{(n+m-1)\times 1} & \boldsymbol{I}^{(n+m-1)\times(n+m-1)}\\ 0 & \boldsymbol{0}^{1\times(n+m-1)}\end{bmatrix} \in \mathbb{R}^{(n+m)\times(n+m)}$, $\boldsymbol{B} \triangleq \begin{bmatrix}\boldsymbol{0}^{1\times(n-1)} & 1 & \boldsymbol{0}^{1\times m}\end{bmatrix}^\top \in \mathbb{R}^{n+m}$, $\boldsymbol{C} \triangleq \begin{bmatrix}1 & \boldsymbol{0}^{1\times(n+m-1)}\end{bmatrix} \in \mathbb{R}^{n+m}$, and $\boldsymbol{H} \triangleq \begin{bmatrix}\boldsymbol{0}^{1\times(n+m-1)} & 1\end{bmatrix}^\top \in \mathbb{R}^{n+m}$.

Remark 2. The reference model may include all available information of the system and disturbances [38]. Therefore, matrices $\boldsymbol{A}_p \in \mathbb{R}^{n\times n}$ and $\boldsymbol{B}_p \in \mathbb{R}^n$ can represent a different linear system from an integrator chain. In this case, $\boldsymbol{A} \triangleq \begin{bmatrix}\boldsymbol{A}_p & \begin{bmatrix}\boldsymbol{B}_p & \boldsymbol{0}^{n\times(m-1)}\end{bmatrix}\\ \boldsymbol{0}^{m\times n} & \bar{\boldsymbol{I}}\end{bmatrix} \in \mathbb{R}^{(n+m)\times(n+m)}$, with $\bar{\boldsymbol{I}} = \begin{bmatrix}\boldsymbol{0}^{(m-1)\times 1} & \boldsymbol{I}^{(m-1)\times(m-1)}\\ 0 & \boldsymbol{0}^{1\times(m-1)}\end{bmatrix} \in \mathbb{R}^{m\times m}$, $\boldsymbol{B} \triangleq \begin{bmatrix}\boldsymbol{B}_p^\top & \boldsymbol{0}^{1\times m}\end{bmatrix}^\top \in \mathbb{R}^{n+m}$, and $\boldsymbol{C} \triangleq \begin{bmatrix}\boldsymbol{C}_p & \boldsymbol{0}^{1\times m}\end{bmatrix} \in \mathbb{R}^{n+m}$. For the sake of simplicity, this paper focuses on models that have the integrator chain form, which is the most common case in ADRC.

To estimate the total disturbance, a full-order generalized proportional integral observer (FOGPIO) is formulated as follows:

$$\dot{\hat{\boldsymbol{x}}}(t) = \boldsymbol{A}\hat{\boldsymbol{x}}(t) + \boldsymbol{B}\kappa_n u(t) + \boldsymbol{L}\left(y(t) - \boldsymbol{C}\hat{\boldsymbol{x}}(t)\right), \tag{4}$$

where $\hat{\boldsymbol{x}} \triangleq [\hat{x}_1 \dots \hat{x}_{n+m}]^\top \in \mathbb{R}^{n+m}$ is the estimate of $\boldsymbol{x}$, and $\boldsymbol{L} \triangleq [l_{n+m-1} \dots l_0]^\top \in \mathbb{R}^{n+m}$ is the observer gain vector.

Estimation error is defined as $\boldsymbol{e}_x(t) = \boldsymbol{x}(t) - \hat{\boldsymbol{x}}(t) \in \mathbb{R}^{n+m}$, and its dynamics is given by

$$\dot{\boldsymbol{e}}_x(t) = \boldsymbol{A}_e\boldsymbol{e}_x(t) + \boldsymbol{H}\xi^{(m)}(t), \tag{5}$$

where $\boldsymbol{A}_e = \boldsymbol{A} - \boldsymbol{L}\boldsymbol{C} \in \mathbb{R}^{(n+m)\times(n+m)}$ is the estimation error matrix, expressed as

$$\boldsymbol{A}_e = \begin{bmatrix}-l_{n+m-1} & 1 & 0 & \cdots & 0\\ -l_{n+m-2} & 0 & 1 & \cdots & 0\\ \vdots & \vdots & \vdots & \ddots & \vdots\\ -l_1 & 0 & 0 & \cdots & 1\\ -l_0 & 0 & 0 & \cdots & 0\end{bmatrix}. \tag{6}$$

The dominant dynamics of the estimation error can be expressed in a polynomial form as follows:

$$p_f(s) = \det(s\boldsymbol{I} - \boldsymbol{A}_e) = s^{n+m} + l_{n+m-1}s^{n+m-1} + \cdots + l_1 s + l_0. \tag{7}$$

thus, if polynomial (7) is Hurwitz, then, the estimation error of FOGPIO remains bounded.

By applying the Laplace transform to Eq. (5), it is possible to find a transfer function vector that relates all estimation errors with the mth derivative of the total disturbance, that is,

$$\frac{\boldsymbol{E}_x(s)}{\Xi_m(s)} = [s\boldsymbol{I} - \boldsymbol{A}_e]^{-1}\boldsymbol{H}. \tag{8}$$

where $\boldsymbol{E}_x(s)$, $\Xi(s)$, and $\Xi_m(s)$ are the Laplace transforms of $\boldsymbol{e}_x(t)$, $\xi(t)$, and $\xi^{(m)}(t)$, respectively. Therefore, $\Xi_m(s) = s^m\Xi(s)$.

Accordingly, the transfer function of any estimation error is given by

$$\frac{E_j(s)}{\Xi_m(s)} = \frac{s^{j-1} + l_{n+m-1}s^{j-2} + \cdots + l_{n+m-j+1}}{s^{n+m} + l_{n+m-1}s^{n+m-1} + \cdots + l_1 s + l_0}, \tag{9}$$

where $E_j(s)$ is the estimation error of state x_j, for $1 \le j \le n+m$. Therefore, the transfer function related to the estimation error of the total disturbance defined as $E_\Xi(s) = \Xi(s) - \hat{\Xi}(s)$ is

$$\frac{E_\Xi(s)}{\Xi_m(s)} = \frac{s^n + l_{n+m-1}s^{n-1} + \cdots + l_m}{s^{n+m} + l_{n+m-1}s^{n+m-1} + \cdots + l_1 s + l_0}. \tag{10}$$

Solving (10) for $\hat{\Xi}(s)$ yields

$$\hat{\Xi}(s) = Q_f(s)\Xi(s), \tag{11}$$

where transfer function $Q_f(s) = \hat{\Xi}(s)/\Xi(s)$, is a filter of relative degree $n+1$ defined as

$$Q_f(s) = \frac{l_{m-1}s^{m-1} + l_{m-2}s^{m-2} + \cdots + l_0}{s^{n+m} + l_{n+m-1}s^{n+m-1} + \cdots + l_1 s + l_0}. \tag{12}$$

2.3. Reduced-order GPIO

Since state $x_1(t)$ is measurable, a reduced-order observer can be used to estimate the remaining $m+n-1$ unknown states. For this purpose, the augmented system (3) can be rewritten as

$$\begin{bmatrix}\dot{x}_m(t)\\ \dot{\boldsymbol{x}}_s(t)\end{bmatrix} = \begin{bmatrix}A_{mm} & \boldsymbol{A}_{ms}\\ \boldsymbol{A}_{sm} & \boldsymbol{A}_{ss}\end{bmatrix}\begin{bmatrix}x_m(t)\\ \boldsymbol{x}_s(t)\end{bmatrix} + \begin{bmatrix}B_m\\ \boldsymbol{B}_s\end{bmatrix}\kappa_n u(t) + \begin{bmatrix}H_m\\ \boldsymbol{H}_s\end{bmatrix}\xi^{(m)}(t), \tag{13}$$

where subscripts m and s denote measured and estimated values, respectively, $x_m(t) = x_1(t)$, and $\boldsymbol{x}_s \triangleq [x_2 \dots x_{n+m}]^\top \in \mathbb{R}^{n+m-1}$. If the reference model is an integrator chain, then, $A_{mm} = B_m = H_m = 0$, $\boldsymbol{A}_{ss} \triangleq \begin{bmatrix}\boldsymbol{0}^{(n+m-2)\times 1} & \boldsymbol{I}^{(n+m-2)\times(n+m-2)}\\ 0 & \boldsymbol{0}^{1\times(n+m-2)}\end{bmatrix} \in \mathbb{R}^{(n+m-1)\times(n+m-1)}$, $\boldsymbol{A}_{sm} \triangleq \boldsymbol{0}^{(n+m-1)\times 1}$, $\boldsymbol{A}_{ms} \triangleq \begin{bmatrix}1 & \boldsymbol{0}^{1\times(n+m-2)}\end{bmatrix} \in \mathbb{R}^{n+m-1}$, $\boldsymbol{B}_s \triangleq \begin{bmatrix}\boldsymbol{0}^{1\times(n-2)} & 1 & \boldsymbol{0}^{1\times m}\end{bmatrix}^\top \in \mathbb{R}^{n+m-1}$, and $\boldsymbol{H}_s \triangleq \begin{bmatrix}\boldsymbol{0}^{1\times(n+m-2)} & 1\end{bmatrix}^\top \in \mathbb{R}^{n+m-1}$.

To formulate a reduced-order GPIO (ROGPIO), the auxiliary vector $\boldsymbol{z}(t) \in \mathbb{R}^{n+m-1}$ is introduced as follows:

$$\boldsymbol{z}(t) = \boldsymbol{x}_s(t) - \boldsymbol{L}_z x_m(t), \tag{14}$$

where $\boldsymbol{L}_z = [\lambda_{n+m-2} \dots \lambda_0]^\top \in \mathrm{R}^{n+m-1}$ is the observer gain vector.

The dynamics of $\boldsymbol{z}(t)$ is given by

$$\begin{aligned}\dot{\boldsymbol{z}}(t) = {} & (\boldsymbol{A}_{sm} - \boldsymbol{L}_z A_{mm})\, x_m(t) + (\boldsymbol{A}_{ss} - \boldsymbol{L}_z\boldsymbol{A}_{ms})\, \boldsymbol{x}_s(t) +\\ & (\boldsymbol{B}_s - \boldsymbol{L}_z B_m)\, \kappa_n u(t) + (\boldsymbol{H}_s - \boldsymbol{L}_z H_m)\, \xi^{(m)}(t).\end{aligned} \tag{15}$$

Therefore, in a simplified form

$$\dot{\boldsymbol{z}}(t) = (\boldsymbol{A}_{ss} - \boldsymbol{L}_z\boldsymbol{A}_{ms})\, \boldsymbol{x}_s(t) + \boldsymbol{B}_s\kappa_n u(t) + \boldsymbol{H}_s\xi^{(m)}(t). \tag{16}$$

By expressing (16) in terms of $y(t) = x_m(t)$, $\boldsymbol{z}(t)$, and $u(t)$, we have

$$\dot{\boldsymbol{z}}(t) = \boldsymbol{A}_z\boldsymbol{z}(t) + \boldsymbol{W}_z y(t) + \boldsymbol{B}_z\kappa_n u(t) + \boldsymbol{H}_z\xi^{(m)}(t), \tag{17}$$

where $\boldsymbol{A}_z = \boldsymbol{A}_{ss} - \boldsymbol{L}_z\boldsymbol{A}_{ms} \in \mathrm{R}^{(n+m-1)\times(n+m-1)}$, $\boldsymbol{B}_z = \boldsymbol{B}_s \in \mathrm{R}^{n+m-1}$, $\boldsymbol{H}_z = \boldsymbol{H}_s \in \mathrm{R}^{n+m-1}$, and $\boldsymbol{W}_z = (\boldsymbol{A}_{ss} - \boldsymbol{L}_z\boldsymbol{A}_{ms})\boldsymbol{L}_z \in \mathrm{R}^{n+m-1}$.

Subsequently, the ROGPIO to estimate $\boldsymbol{z}(t)$ is designed as

$$\dot{\hat{\boldsymbol{z}}}(t) = \boldsymbol{A}_z\hat{\boldsymbol{z}}(t) + \boldsymbol{B}_z\kappa_n u(t) + \boldsymbol{W}_z y(t), \tag{18}$$

where $\hat{\boldsymbol{z}} = [\hat{z}_1 \dots \hat{z}_{n+m-1}]^\top \in \mathbb{R}^{n+m-1}$ represents the estimate of $\boldsymbol{z}$, and the unknown state vector is determined by

$$\hat{\boldsymbol{x}}_s(t) = \hat{\boldsymbol{z}}(t) + \boldsymbol{L}_z y(t). \tag{19}$$

Since $\boldsymbol{e}_z(t) = \boldsymbol{z}(t) - \hat{\boldsymbol{z}}(t)$ equals $\boldsymbol{e}_s(t) = \boldsymbol{x}_s(t) - \hat{\boldsymbol{x}}_s(t)$, thus, the estimation error dynamics of ROGPIO is given by

$$\dot{\boldsymbol{e}}_s(t) = \boldsymbol{A}_z\boldsymbol{e}_s(t) + \boldsymbol{H}_z\xi^{(m)}(t), \tag{20}$$

where $\boldsymbol{e}_s = [e_{x2} \dots e_{x(n+m)}]^\top \in \mathbb{R}^{n+m-1}$, and

$$\boldsymbol{A}_z = \begin{bmatrix}-\lambda_{n+m-2} & 1 & 0 & \cdots & 0\\ -\lambda_{n+m-3} & 0 & 1 & \cdots & 0\\ \vdots & \vdots & \vdots & \ddots & \vdots\\ -\lambda_1 & 0 & 0 & \cdots & 1\\ -\lambda_0 & 0 & 0 & \cdots & 0\end{bmatrix}. \tag{21}$$

If $\boldsymbol{A}_z$ is Hurwitz and $\sup_t |\xi^{(m)}(t)| \leq \epsilon_m$, then, it can be established that $\boldsymbol{e}_s(t)$ remains bounded. In addition, the characteristic polynomial of the ROGPIO can be expressed as

$$p_r(s) = s^{n+m-1} + \lambda_{n+m-2}s^{n+m-2} + \cdots + \lambda_1 s + \lambda_0. \tag{22}$$

By Applying the Laplace transform to (20), we have

$$\frac{\bar{\boldsymbol{E}}_s(s)}{\Xi_m(s)} = [s\boldsymbol{I} - \boldsymbol{A}_z]^{-1}\boldsymbol{H}_z. \tag{23}$$

The transfer function of any estimation error is

$$\frac{\bar{E}_j(s)}{\Xi_m(s)} = \frac{s^{j-2} + \lambda_{n+m-2}s^{j-3} + \cdots + \lambda_{n+m-j+1}}{s^{n+m-1} + \lambda_{n+m-2}s^{n+m-2} + \cdots + \lambda_1 s + \lambda_0}, \tag{24}$$

where $\bar{E}_j(s)$ is the estimation error of state x_j, for $2 \leq j \leq n+m$.

The estimate of the total disturbance in the ROGPIO is given by

$$\hat{\Xi}(s) = Q_r(s)\Xi(s), \tag{25}$$

where transfer function $Q_r(s) = \hat{\Xi}(s)/\Xi(s)$ is a filter of relative degree n, which satisfies

$$Q_r(s) = \frac{\lambda_{m-1}s^{m-1} + \lambda_{m-2}s^{m-2} + \cdots \lambda_0}{s^{n+m-1} + \lambda_{n+m-2}s^{n+m-2} + \cdots + \lambda_1 s + \lambda_0}. \tag{26}$$

Filters (12) and (26) can be used to establish equivalence relations between GPIO and the frequency-domain disturbance observer, which is explained below.

2.4. Frequency-domain DOB

Time-domain formation of GPIO is able to estimate both the system states and the total disturbance. However, from the viewpoint of the inner loop, only the disturbance is necessary. Let us introduce an input–output representation of (2) as follows:

$$y^{(n)}(t) = \kappa_n u(t) + \xi(t). \tag{27}$$

Then, it is possible to solve $\xi(t)$ from (27) as

$$\xi(t) = y^{(n)}(t) - \kappa_n u(t). \tag{28}$$

By applying the Laplace transform and taking initial conditions equal to 0, we have

$$\Xi(s) = s^n Y(s) - \kappa_n U(s). \tag{29}$$

where $\Xi(s)$, $Y(s)$, and $U(s)$ are the Laplace transforms of $\xi(t)$, $y(t)$, and $u(t)$, respectively.

Since Eq. (29) is not implementable due to the explicit derivatives on the output, a low-pass filter of relative degree greater than or equal to n, denoted as $Q_d(s)$ and commonly called the Q-filter, is introduced as follows:

$$\hat{\Xi}(s) = Q_d(s)\Xi(s) = Q_d(s)s^n Y(s) - Q_d(s)\kappa_n U(s), \tag{30}$$

where $\hat{\Xi}(s)$ is the estimate of the total disturbance. Note that equation (30) agrees with the frequency-domain formulation of the disturbance observer (DOB).

Remark 3. Disturbance estimation provided by DOB in Eq. (30) is equivalent to that obtained by FOGPIO, if and only if, the Q-filter has the structure presented in (12), i.e., $Q_d(s) = Q_f(s)$. Similarly, if $Q_d(s) = Q_r(s)$, according to (26), then, DOB is equivalent to ROGPIO. It is worth noting that this equivalence also clarifies the concept of extended state (m) in the frequency-domain DOB.

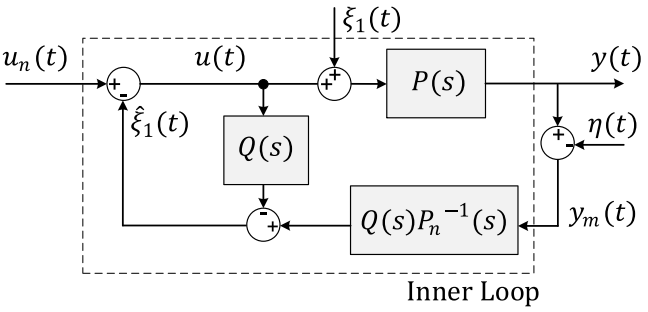

Fig. 2. Inner loop of GPIO-based control in frequency-domain.

2.5. Q-filters for ESO and RESO

Results obtained for GPIO can be applied to extended state observer (ESO). Therefore, if the total disturbance is modeled as $d\xi(t)/dt = 0$ ($m = 1$), which is common in ADRC design, the equivalent Q-filter of a full-order ESO is obtained from (12) as follows:

$$Q_{f1}(s) = \frac{l_0}{s^{n+1} + l_n s^n + \cdots + l_1 s + l_0}. \tag{31}$$

In the same way, from (26) the Q-filter of a reduced-order ESO (RESO) is equal to

$$Q_{r1}(s) = \frac{\lambda_0}{s^n + \lambda_{n-1}s^{n-1} + \cdots + \lambda_1 s + \lambda_0}. \tag{32}$$

As mentioned before, the equivalence between GPIO and DOB can be established in terms of Q-filters under a frequency-domain framework. This will be used below to perform a robustness and performance analysis of GPIO.

3. Robustness and performance analysis of GPIO

In this section, several analyses of GPIO are performed with a frequency-domain approach. First, the transfer functions concerning the disturbance rejection stage are deduced. Next, the influence is analyzed of the system order, the number of extended states, the uncertain control gain, and the tuning method on the robustness and performance of GPIO.

3.1. Transfer functions of the disturbance rejection stage

Fig. 2 shows the block diagram corresponding to the inner loop of a GPIO-based control. Inspired by the DOB formulation, the filter associated to the observer is denoted as $Q(s)$, the input equivalent disturbance is $\Xi_1(s)$, the real plant is $P(s)$, and the reference (nominal) model is $P_n(s)$. Since stability margins have no dependence on the initial conditions of the states, it is valid to assume them equal to zero to perform a robustness analysis. Therefore, in line with Section 2, the reference model (integrator chain) in frequency-domain is expressed as follows:

$$P_n(s) = \frac{\kappa_n}{s^n}, \tag{33}$$

where n is the system order, κ_n represents the nominal control gain, and the total disturbance is $\Xi_1(s) = \Xi(s)/\kappa_n$.

Accordingly, the estimate of $\Xi_1(s)$ is defined as

$$\hat{\Xi}_1(s) = Q(s)P_n^{-1}(s)Y(s) - Q(s)U(s), \tag{34}$$

where $Q(s)$ can take the form of FOGPIO, ROGPIO, ESO, and RESO, whose structures are presented in Eqs. (12), (26), (31), and (32), respectively.

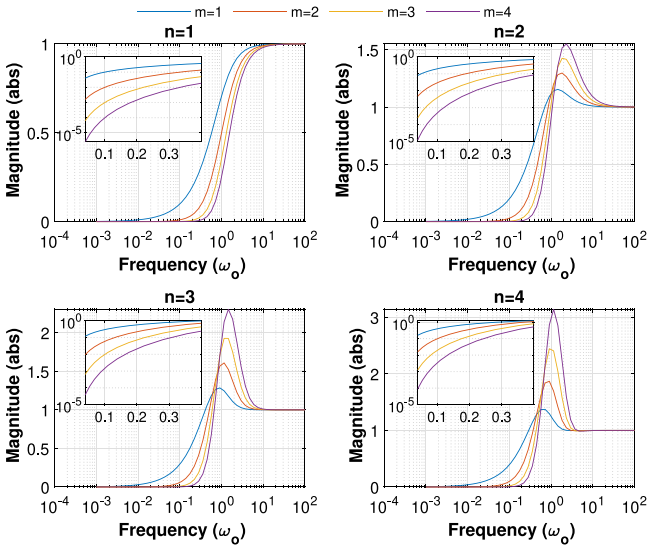

Fig. 3. Sensitivity of ROGPIO for $n \in [1, 4]$, $m \in [1, 4]$, $\Delta_\kappa = 1$, and bandwidth ω_o. Close-ups diagrams are in log-scale.

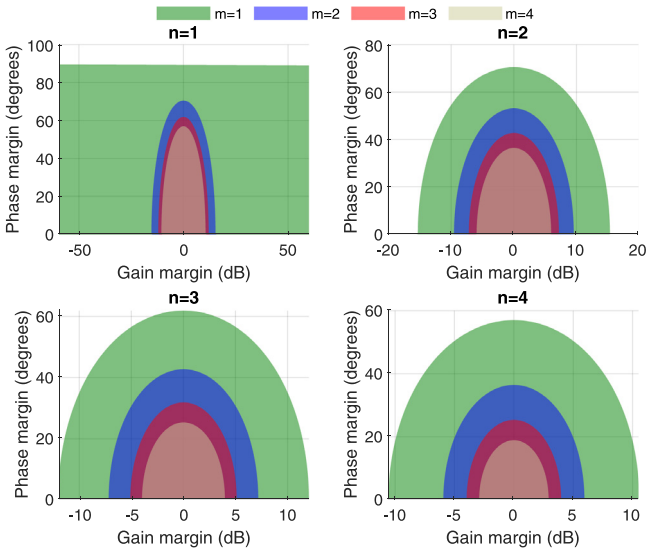

Fig. 4. Balanced disk-based margins of ROGPIO for $n \in [1, 4]$ and $m \in [1, 4]$.

Taking into account the influence of control gain on stability of ESO-based ADRC [28], it results convenient to analyze this effect on GPIO. Therefore, the uncertainty on control gain is defined as

$$\Delta_\kappa = \frac{\kappa}{\kappa_n}. \tag{35}$$

Using block diagram 2 and Eqs. (33) to (35), the transfer functions of loop $L(s)$, sensitivity $S(s)$, and complementary sensitivity $T(s)$ are written as follows:

$$L(s) = \frac{\Delta_\kappa Q(s)}{1 - Q(s)}, \tag{36}$$

$$S(s) = \frac{\Xi_1(s) - \hat{\Xi}_1(s)}{\Xi_1(s)} = \frac{1 - Q(s)}{1 - (1 - \Delta_\kappa)Q(s)}. \tag{37}$$

$$T(s) = \frac{\hat{\Xi}_1(s)}{\Xi_1(s)} = \frac{\Delta_\kappa Q(s)}{1 - (1 - \Delta_\kappa)Q(s)}. \tag{38}$$

A basic analysis for $\Delta_\kappa = 1$, reveals that the nominal sensibility and complementary sensitivity are $S_n(s) = 1 - Q(s)$, and $T_n(s) = Q(s)$, respectively. These results suggest that $S_n(s)$ must be minimal at low frequencies for disturbance attenuation, whereas $Q(s)$ should tend to 0 at high frequencies to improve robustness and noise rejection.

Although previous considerations constitute a starting point to analyze the GPIO in the frequency-domain, they provide no deeper insights. Therefore, next subsections present further performance and robustness analyses of GPIO.

3.2. Number of extended states

To understand the effect of the number of extended states on the robustness of ROGPIO, the sensitivity $S(s)$, and the complementary sensitivity $T(s)$ functions are analyzed for $\Delta_\kappa = 1$ and changing the system order. Fig. 3 shows the frequency-response of $S(s)$ for $n \in [1, 4]$ and $m \in [1, 4]$, where the observer bandwidth is denoted as ω_o, and the characteristic polynomial has the following binomial form [28,39]:

$$p_o(s) = (s + \omega_o)^{n+m-1}. \tag{39}$$

From a qualitative point of view, results in Fig. 3 show that the maximum sensitivity peak, denoted as $M_S = \|S(j\omega)\|_\infty$, increases with both the system order and the number of extended states. This indicator is a measure of the worst-case performance degradation, which occurs at intermediate frequencies. Likewise, M_S has an influence on robustness due to its relationship with the phase margin (PM_S) and the gain margin (GM_S) [40], since

$$PM_S \geq \frac{360}{\pi} \arcsin\left(\frac{1}{2M_S}\right) \quad \text{(deg)}, \tag{40}$$

$$GM_S \geq \frac{M_S}{M_S - 1} \quad \text{(abs)}. \tag{41}$$

From a quantitative perspective, Table 3 summarizes the classical performance and robustness measures of ROGPIO. With respect to robustness, PM_S, and GM_S are reduced when m increases, except for first-order plants, in which the margins remain constant, at least from the point of view of M_S. For high-order plants, these robustness measures also decrease, which coincides with a larger M_S. Finally, GM_S can be used as a measure of the maximum range of the uncertain control gain. This range is studied in depth in the next subsection.

Regarding performance, the bandwidth of $S(s)$ denoted as ω_S is enhanced by increasing m for any system order. In addition, for $n > 1$, $\omega_S < \omega_O$; thus, ω_S becomes a practical index of the disturbance rejection performance. This fact, explains that it is mandatory to increase the observer bandwidth to reduce the estimation error using fewer extended states. However, this increase can boost the effects of measurement noise.

As regards the bandwidth of $T(s)$ denoted as ω_T, it is also expanded when m increases, which produces a wider noise-sensitivity range defined as $\omega_N = \omega_T - \omega_S$. This effect occur because sensitivity peak M_S at ω_{M_S}, and complementary sensitivity peak M_T at ω_{M_T} are within the interval $[\omega_S, \omega_T]$ [40]. Accordingly, noise amplification and reduction in stability margins become the main practical limitations of high-order GPIO.

3.3. Uncertain control gain

An important scenario for the robustness analysis of ROGPIO is the capability to handle the uncertainty on control gain [28]. Consequently, in this subsection disk-based margins (DM) are used to quantify the stability against combined gain and phase variations [41]. In this context, Fig. 4 presents the disk-based gain margins (DGM) and the disk-based phase margins (DPM)

Table 3
Classical performance and robustness measures of ROGPIO.

n	m	Margins		Sensitivity			Complementary sensitivity			$\omega_N(\omega_o)$
		PM (deg)	GM (abs)	$\omega_S(\omega_o)$	M_S (abs)	$\omega_{M_S}(\omega_o)$	$\omega_T(\omega_o)$	M_T (abs)	$\omega_{M_T}(\omega_o)$	
1	1	60	∞	1.000	1	–	1.00	1	0	0
	2	60	∞	1.5538	1	–	2.4785	1.1547	0.7019	0.9248
	3	60	∞	1.9615	1	–	3.8934	1.2857	1.1534	1.9319
	4	60	∞	2.2990	1	–	5.2915	1.3809	1.5386	2.9925
2	1	51.3333	7.4777	0.4028	1.1544	1.3653	0.6423	1	0	0.2395
	2	45.2751	4.3441	0.6089	1.2990	1.7335	1.6409	1.2990	0.5769	1.0320
	3	40.9034	3.3204	0.7526	1.4310	1.9727	2.5288	1.6114	0.9115	1.7762
	4	37.5675	2.8089	0.8677	1.5528	2.2460	3.3856	1.8835	1.1954	2.5179
3	1	45.7708	4.5000	0.2565	1.2857	0.8643	0.5088	1	0	0.2524
	2	36.1540	2.6357	0.3951	1.6114	1.0923	1.3278	1.4311	0.4986	0.9326
	3	29.6670	2.0493	0.4955	1.9530	1.2827	2.0171	1.9531	0.7721	1.5216
	4	25.0776	1.7674	0.5776	2.3031	1.4564	2.6683	2.4749	1	2.0907
4	1	42.4572	3.6256	0.1887	1.3809	0.6499	0.4342	1	0	0.2454
	2	30.7895	2.1319	0.2951	1.8835	0.8365	1.1518	1.5528	0.4459	0.8566
	3	23.3114	1.6780	0.3746	2.4749	1.000	1.7306	2.3031	0.6815	1.3560
	4	18.3249	1.4663	0.4408	3.1400	1.1458	2.2677	3.1400	0.8727	1.8269

Table 4
Balanced disk-based margins of ROGPIO.

n	m	DPM (deg)	DGM (abs)	
		Max	$\Delta_\kappa$min	$\Delta_\kappa$max
1	1	90.0	0	∞
	2	70.5	0.172	5.83
	3	61.9	0.250	4.00
	4	57.0	0.296	3.37
2	1	70.5	0.172	5.83
	2	53.1	0.333	3.00
	3	42.7	0.438	2.29
	4	36.4	0.505	1.98
3	1	61.9	0.250	4.00
	2	42.7	0.438	2.29
	3	31.9	0.556	1.80
	4	25.4	0.633	1.58
4	1	57.0	0.296	3.37
	2	36.4	0.505	1.98
	3	25.4	0.633	1.58
	4	18.9	0.714	1.40

Table 5
Maximum range of uncertainty on control gain ($\Delta_\kappa \min_t$, $\Delta_\kappa \max_t$) of ROGPIO for $n \in [1, 4]$ and $m \in [1, 4]$.

$n \setminus m$	1	2	3	4
1	$(0, \infty)$	$(0.12, \infty)$	$(0.20, \infty)$	$(0.26, \infty)$
2	$(0, 9.32)$	$(0.18, 5.83)$	$(0.33, 4.79)$	$(0.43, 4.28)$
3	$(0, 5.00)$	$(0.21, 3.07)$	$(0.41, 2.46)$	$(0.54, 2.16)$
4	$(0, 3.89)$	$(0.24, 2.33)$	$(0.47, 1.85)$	$(0.62, 1.63)$

of ROGPIO. These margins are computed from the loop function (36), for different values of n and m, using the characteristic polynomial (39).

Shaded regions in Fig. 4 represent the stable range of balanced gain and phase changes for all frequencies. Table 4 summarizes the influence of n and m on DGM and DPM, which reveals two elements. First, DGM not only defines a lower bound for Δ_κ, which is not given by GM_S, but also provides a more practical and reliable measure of how much the control gain can increase or decrease without loss of stability. Second, DPM defines the maximum phase variation, thus complementing the one given by PM_S (the worst case).

Even though insights presented in Fig. 4 and Table 4 are useful for practical purposes, the results derived from balanced disk-margin may seem conservative from a theoretical viewpoint. Therefore, it is possible to compute unbalanced disk margins to find the maximum range of Δ_κ that the inner loop can tolerate.

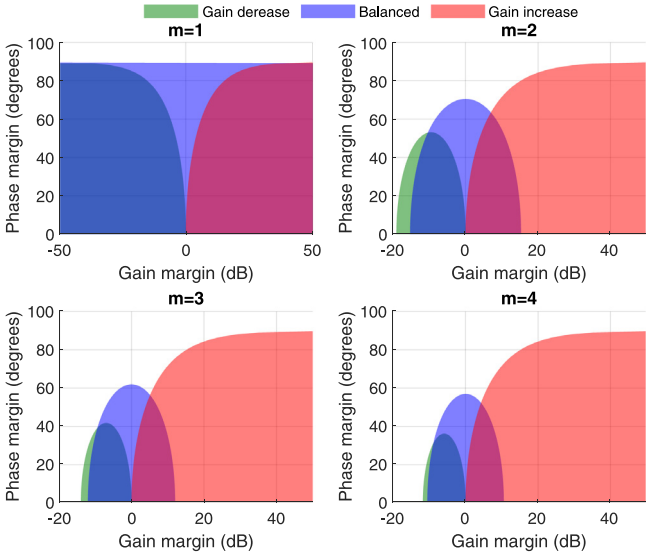

Fig. 5. Unbalanced disk-based margins of ROGPIO for $n = 1$ and $m \in [1, 4]$. (For interpretation of the references to color in this figure legend, the reader is referred to the web version of this article.)

Figs. 5 to 8 depict the unbalanced disk margins for different system orders. To compare the relative sensitivity, tree cases are considered: (1) the balanced case (blue), (2) larger gain decrease than increase (green), and (3) larger gain increase than decrease (red).

Table 5 presents the maximum theoretical ranges of uncertainty on control gain denoted as ($\Delta_\kappa \min_t$, $\Delta_\kappa \max_t$). In general terms, these ranges are wider than those presented in Table 4. Unbalanced disk margins reveal that the inner loop is more sensitive to gain increase for $n < m$, whereas the loop stability is more sensitive to gain decrease when $n > m$. Additionally, the sensitivity for $n = m$ is approximately symmetrical in terms of gain variations.

Remark 4. Table 5 shows that the tolerable range of the uncertain control gain decreases with both n and m. Consequently, it is advisable to start tuning with the fewest extended states in cases of high-order plants, time-varying $\kappa(t)$, or highly uncertain systems.

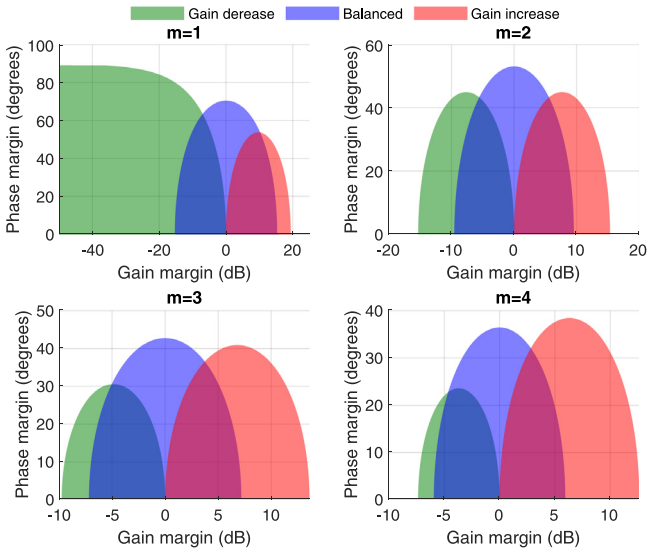

Fig. 6. Unbalanced disk-based margins of ROGPIO for $n = 2$ and $m \in [1, 4]$. (For interpretation of the references to color in this figure legend, the reader is referred to the web version of this article.)

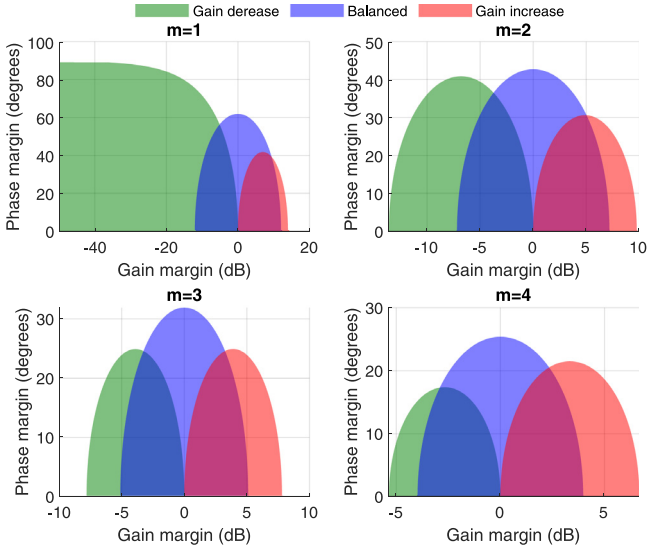

Fig. 7. Unbalanced disk-based margins of ROGPIO for $n = 3$ and $m \in [1, 4]$. (For interpretation of the references to color in this figure legend, the reader is referred to the web version of this article.)

Remark 5. According to Table 5, when the observer has a single extended state ($m = 1$), not only the robustness is the highest, but also the lower bound of Δ_κ tends to zero. This feature explains the wide acceptance of ESO despite its lower effective bandwidth, as shown in Table 3.

Remark 6. Disk margins quantify the robustness of the inner loop against control gain variations caused by either modeling errors or changes in system components. However, in practice, if the system is able to operate, then, the uncertainties will be absorbed by the total disturbance. Therefore, when stability is guaranteed, the steady-state estimation error is the one expected for the nominal case (Fig. 3).

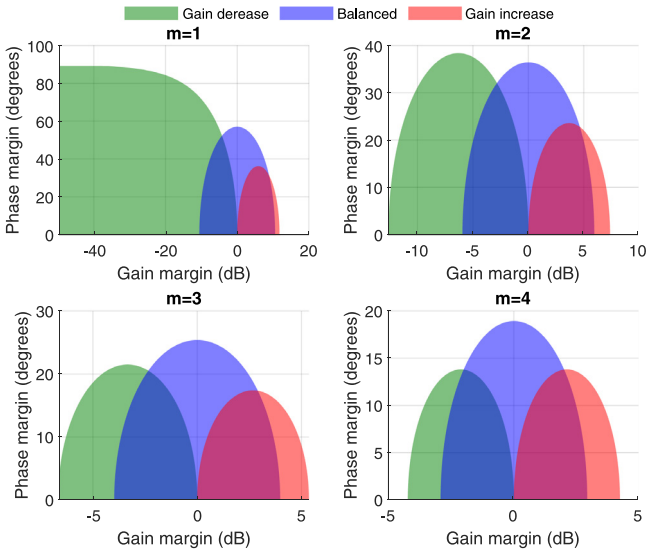

Fig. 8. Unbalanced disk-based margins of ROGPIO for $n = 4$ and $m \in [1, 4]$. (For interpretation of the references to color in this figure legend, the reader is referred to the web version of this article.)

3.4. Comparison of basic tuning methods

To make a fair comparison among different tuning methods, it results convenient to use a weighted sensitivity, denoted as $W_d(s)S(s)$, since it is a good indicator of performance and robustness [40]. Additionally, typical specifications in the frequency-domain can be captured by an upper bound on the magnitude of $S(s)$, such that

$$|S(j\omega)| \leq 1/\left|W_d(j\omega)\right|, \forall j\omega, \tag{42}$$

where $W_d(s)$ is a weight function that includes the desired bandwidth ω_d, the maximum steady-state estimation error A_d, and the maximum sensitivity peak M_d. As mentioned above, a certain $\|S(ju)\|_\infty \leq M_d$ is required in order to prevent noise amplification at high frequencies, and guarantee the desired stability margins, which can be adjusted using Eqs. (40) and (41). Consequently, in this work the following first-order weight function is adopted:

$$W_d(s) = \frac{s/M_d + \omega_d}{s + A_d\omega_d}. \tag{43}$$

From (42), it is clear that to comply with the requirements, the condition $\|W_d(j\omega)S(j\omega)\|_\infty \leq 1$ must be guaranteed. This indicator facilitates the comparison of basic tuning methods scaled by the observer bandwidth ω_o, such as (1) binomial tuning [39], (2) optimal polynomials in sense of ITAE criteria [42], and (3) Bessel polynomials [43]. Accordingly, Fig. 9 presents the weighted sensitivity for the three methods using $M_d = 2.06$ ($PM \geq 28°$, $GM \geq 1.95$), $A_d = 1 \times 10^{-3}$, and $\omega_d = \omega_o$, which are reasonable frequency-domain specifications.

Results derived from binomial tuning reaffirm those presented in Fig. 3 and Table 3, where the effective bandwidth is less than ω_o, except for first-order plants. In addition, a performance improvement can be observed by increasing m, but without achieving compliance with the specifications. In contrast, ITAE tuning is characterized by a greater bandwidth, and a reduction of M_S in most cases. Bessel tuning produces the required results for $n \in [1, 2]$ and $m \in [1, 3]$, as well as an improvement in the other cases. This is due to some features of Bessel filters, such as an almost constant group delay in the pass-band, and a slow transition to the stop-band [43].

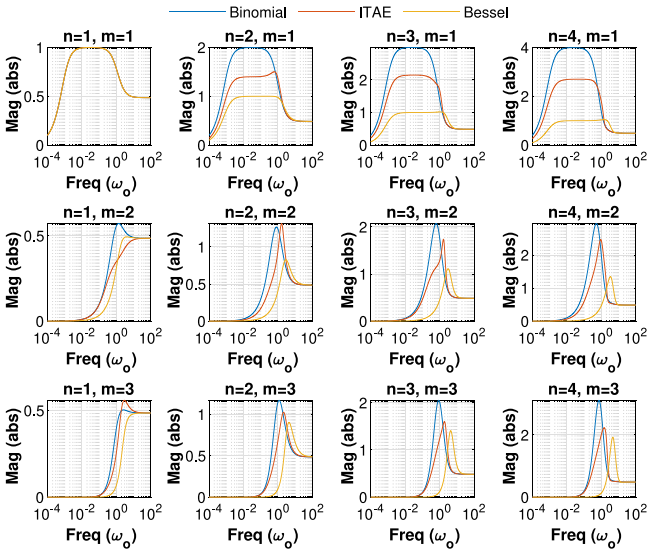

Fig. 9. Weighted sensitivity for different tuning methods using $\omega_o = \omega_d$.

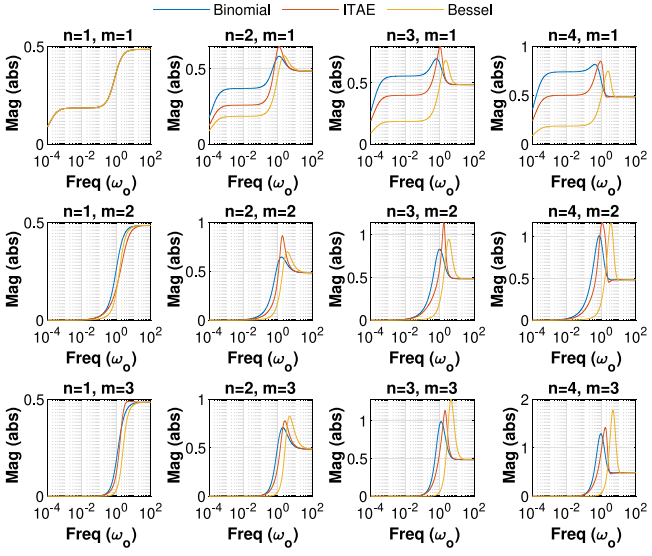

Fig. 10. Weighted sensitivity for different tuning methods using $\omega_o = 5.4\omega_d$.

Remark 7. According to Table 3, binomial tuning of ROGPIO has robustness restrictions, which depend on n and m. However, if the stability margins satisfy the requirements, then, it is possible to determine the proper observer bandwidth to accomplish the remaining specifications. For this purpose, ω_o must be adjusted according to the value of ω_S presented in Table 3, such that, $\omega_o > \omega_d/\omega_S$. For instance, when $M_S = 2.06$ and $\omega_o = 5.4\omega_d$ all requirements are met for $n \in [1, 3]$ and $m \in [1, 3]$ as well as for $n = 4$ and $m \in [1, 2]$, as shown in Fig. 10. This procedure can be used as a guideline for the other basic tuning methods.

4. Comparison between ROGPIO and FOGPIO

In this section, a comparison between FOGPIO and ROGPIO is presented in the frequency-domain. To perform the analysis, the control system depicted in Fig. 11, which includes both inner and outer loop, is considered.

4.1. Inner loop

Both ROGPIO and FOGPIO can be described in terms of a Q-filter, by using the equivalence presented in Section 2. In fact, $Q_f(s)$ for FOGPIO, and $Q_r(s)$ for ROGPIO have the special form presented in Eqs. (12) and (26), respectively. Consequently, the proposed analysis can be applied to extract the main robustness and performance measures of FOGPIO, which are summarized in Table 6.

Results show that for any combination of system order and number of extended states, the robustness margins of FOGPIO are fewer than in ROGPIO. The sensitivity bandwidth ω_S and the tolerable range of uncertain control gain ($\Delta_\kappa$min, $\Delta_\kappa$max), are also smaller. In contrast, FOGPIO presents a narrower noise-sensitivity range $\omega_N = \omega_T - \omega_S$ for $n > 1$. This advantage can motivate the practical use of FOGPIO in spite of its lower robustness.

Remark 8. There is a relation between the Q-filters of FOGPIO and ROGPIO for any n and m, which satisfies

$$Q_f(s)\Big|_{n,m} = Q_r(s)\Big|_{(n+1),m}. \tag{44}$$

4.2. Outer loop: ADRC approach

The objective of implementing an inner loop based on disturbance rejection is to impose a reference model that can be controlled by any kind of feedback regulator. However, since GPIO is commonly used in ADRC designs, it is worth comparing the performance and robustness of ROGPIO and FOGPIO under such framework. Let us define the following control law for system (2):

$$u(t) = \frac{u_n(t) - \xi(t)}{\kappa_n}, \tag{45}$$

where $u_n(t)$ is the nominal control provided by the outer loop.

Next, consider a feed-forward nominal controller that uses the estimated states as follows:

$$u_n(t) = y^*(t)^{(n)} - k_0\left(y(t) - y^*(t)\right) - \sum_{j=2}^{n} k_{j-1}\left(\hat{x}_j(t) - y^*(t)^{(j-1)}\right). \tag{46}$$

where $[k_{n-1} \cdots k_0]$ are the outer loop design parameters.

If a stable inner loop is guaranteed, then, the uncertainty related to control gain is lumped into the total disturbance. In consequence, the estimation errors $e_j(t) = x_j(t) - \hat{x}_j(t)$ for $j \in [2, n+m]$ remain bounded, and they converge to their nominal values. Therefore, the tracking error defined as $\varepsilon_y(t) = y(t) - y^*(t)$ has the following time-domain dynamics:

$$\varepsilon_y^{(n)}(t) + \sum_{j=0}^{n-1} k_j \varepsilon_y^{(j)}(t) = \xi(t) - \hat{\xi}(t) + \sum_{j=2}^{n} k_{j-1} e_j(t). \tag{47}$$

By applying the Laplace transform to (47) and assuming initial conditions equal to zero, we obtain

$$p_y(s)E_y(s) = S(s)\Xi(s) + \sum_{j=2}^{n} k_{j-1}E_j(s), \tag{48}$$

where $E_y(s)$ ans $E_j(s)$ are the Laplace transforms of $\varepsilon_y(t)$ and $e_j(t)$, respectively, $S(s) = 1 - Q(s)$, is the nominal inner loop sensitivity, and $Q(s)$ is the equivalent Q-filter according to (12) and (26). Additionally, the polynomial containing the eigenvalues of the tracking controller is

$$p_y(s) = s^n + k_{n-1}s^{n-1} + \cdots + k_1 s^1 + k_0 s^0. \tag{49}$$

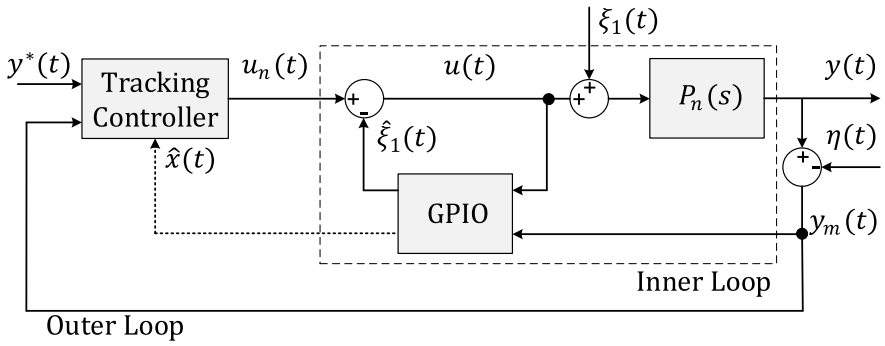

Fig. 11. Block diagram of GPIO-based control.

Table 6
Robustness and performance measures of FOGPIO.

n	m	Phase margin (deg)		Gain margin (abs)		Frequencies (ω_o)		
		PM	*DPM*	*GM*	($\Delta_\kappa \min_t$, $\Delta_\kappa \max_t$)	ω_S	ω_T	ω_N
1	1	51.3333	70.5	7.4777	(0,9.32)	0.4028	0.6423	0.2395
	2	45.2751	53.1	4.3441	(0.172,5.83)	0.6089	1.6409	1.0320
	3	40.9034	42.7	3.3204	(0.326,4.79)	0.7526	2.5288	1.7762
	4	37.5675	36.4	2.8089	(0.429,4.28)	0.8677	3.3856	2.5179
2	1	45.7708	61.9	4.5000	(0,5.00)	0.2565	0.5088	0.2524
	2	36.1540	42.7	2.6357	(0.209,3.07)	0.3951	1.3278	0.9326
	3	29.6670	31.9	2.0493	(0.407,2.46)	0.4955	2.0171	1.5216
	4	25.0776	25.4	1.7674	(0.54,2.16)	0.5776	2.6683	2.0907
3	1	42.4572	57.0	3.6256	(0,3.89)	0.1887	0.4342	0.2454
	2	30.7895	36.4	2.1319	(0.234,2.33)	0.2951	1.1518	0.8566
	3	23.3114	25.4	1.6780	(0.464,1.85)	0.3746	1.7306	1.3560
	4	18.3249	18.9	1.4673	(0.615,1.63)	0.4408	2.2677	1.8269
4	1	40.2570	53.7	3.2077	(0,3.37)	0.1494	0.3849	0.2355
	2	27.2704	32.2	1.8921	(0.252,2.00)	0.2363	1.0350	0.7987
	3	19.2805	21.1	1.5036	(0.505,1.59)	0.3026	1.5417	1.2391
	4	14.2153	14.8	1.3288	(0.667,1.41)	0.3588	2.0047	1.6460

Finally, the tracking error satisfies

$$E_y(s) = G(s)\Xi(s), \tag{50}$$

where $G(s)$ is the sensitivity function of the outer loop defined as follows:

$$G(s) = \frac{1}{p_y(s)}\left[1 - Q(s) + \sum_{j=2}^{n} k_{j-1} s^m \frac{E_j(s)}{\Xi_m(s)}\right], \tag{51}$$

and transfer functions $E_j(s)/\Xi_m(s)$ can be computed from Eqs. (9) and (24).

Remark 9. Since FOGPIO also provides an estimate of the measured output ($\hat{x}_1(t) = \hat{y}(t)$), it can be used to implement an alternative control law as follows:

$$u_n(t) = y^*(t)^{(n)} - \sum_{j=1}^{n} k_{j-1}\left(\hat{x}_j(t) - y^*(t)^{(j-1)}\right). \tag{52}$$

As a result, the corresponding sensitivity function of the outer loop is

$$G(s) = \frac{1}{p_y(s)}\left[1 - Q_f(s) + \sum_{j=1}^{n} k_{j-1} \frac{s^m E_j(s)}{\Xi_m(s)}\right]. \tag{53}$$

Although control law (52) increases the tracking error, the use of $x_1(t)$ instead of $y(t)$, has a filtering effect, which can be useful for high-order observers. In addition, for designs based on FOGPIO, $e_1(t)$ can be used either as a measurable indicator of the estimation process or as an insight for an online tuning strategy.

Remark 10. Note that if the nominal model is selected as $P_n(s) = \kappa_n/s^n$, then, the equivalent input disturbance has the form $\Xi_1(s) = \Xi(s)/\kappa_n$. Such consideration allows analyzing the effect of a total disturbance in the same order of magnitude as the control signal. In that case, the tracking error is defined as

$$E_y(s) = \kappa_n G(s)\Xi_1(s). \tag{54}$$

Fig. 12 shows the sensitivity of the outer loop for FOGPIO with $\hat{x}_1(t)$, FOGPIO with $y(t)$, and ROGPIO. In this case, $\kappa_n = 1$ and $p_y(s) = (s+\omega_c)^n$, where ω_c is the outer loop bandwidth assumed here as $\omega_c = \omega_o/3$. Results show that ROGPIO has the smallest tracking error and sensitivity peak in all cases and its effective bandwidth is always the largest.

5. Experimental validation

To validate the results presented in Sections 2, 3, and 4, the voltage control for a synchronous buck converter is considered below.

5.1. System description

A synchronous buck converter (SBC) is a power interface comprised of a low-pass LC filter, the load resistance, and two electronic switches (Q1 and Q2) that are controlled by PWM. The circuit scheme of a SBC is presented in Fig. 13. Although this converter is a nonlinear and hybrid dynamic system, it is often modeled using a simplified average model [44,45] as follows:

$$L\frac{di_l(t)}{dt} = -v_c(t) + u(t)v_i(t), \qquad C\frac{dv_c(t)}{dt} = -\frac{v_c(t)}{R} + i_l(t), \tag{55}$$

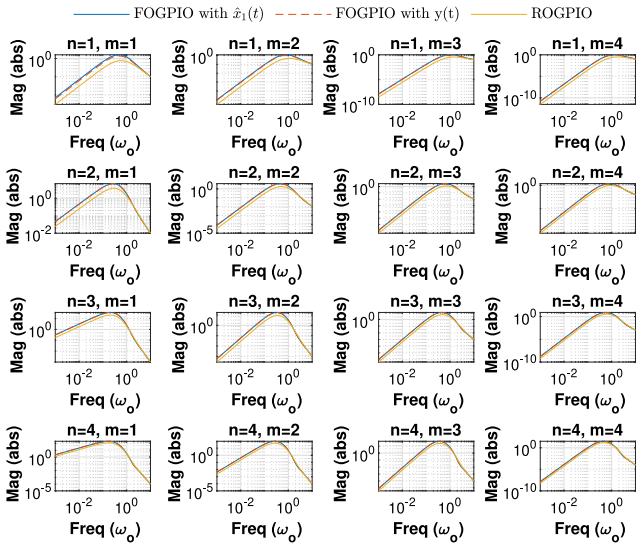

Fig. 12. Outer loop sensitivity for $n \in [1, 4]$, $m \in [1, 4]$, and $\omega_c = \omega_o/3$.

where L, C and R are the inductance, capacitance and load resistance, respectively. $v_c(t)$ and $i_l(t)$ are the averages of the capacitor voltage and the inductor current. Additionally, $v_i(t)$ is the input voltage, and duty cycle $u(t) \in [0, 1]$ represents the control signal.

During its operation, the SBC can be disturbed by variations in the input voltage and the load [46]. Likewise, L and C can suffer changes that cause uncertainty in output voltage regulation [45]. Furthermore, there are different unmodeled dynamics such as power losses, switching dead time, magnetic restriction in the inductor, and electromagnetic interference, which are assumed as part of the total disturbance [44]. Due to these characteristics, schemes based on disturbance rejection are useful to control this type of systems [47].

Regarding control of buck converters, it is possible to use either current or voltage feedback. However voltage-mode control is often used not only due to its low open-loop output impedance, but also in order to suppress the inductor current sensor [44,48]. Therefore, defining $v_o(t) = v_c(t)$ as the output, model (55) is rewritten as follows:

$$\frac{d^2 v_o(t)}{dt^2} = \frac{1}{LC} u(t) v_i(t) - \frac{1}{LC} v_o(t) - \frac{1}{RC} \frac{dv_o(t)}{dt}. \tag{56}$$

Form Eq. (56) the SBC can be modeled by the following disturbed integrator chain:

$$\frac{d^2 v_o(t)}{dt^2} = \kappa(t) u(t) + \xi(t), \tag{57}$$

where $\kappa(t) = \frac{v_i(t)}{LC}$, $\xi(t) = -\frac{1}{LC} v_o(t) - \frac{1}{RC} \frac{dv_o(t)}{dt} + \zeta(t)$, and $\zeta(t)$ denotes any unknown external disturbance, uncertainty, or unmodeled dynamics.

The control problem for system (57) is formulated as follows: find a control law such that the output voltage $v_o(t)$ tracks the reference path $v_o^*(t)$, even in presence of changes in the load and input voltage variations. To achieve this objective, the control system depicted in Fig. 11 is considered.

If initial conditions are assumed equal to zero, and $\bar{C}$, $\bar{L}$, and $\bar{V}_i$ are the nominal circuit values, then the frequency-domain reference model is defined as

$$P_n(s) = \frac{V_o(s)}{U(s) + \Xi_1(s)} = \frac{\kappa_n}{s^2} = \frac{\bar{V}_i/\bar{L}\bar{C}}{s^2}, \tag{58}$$

where $\kappa_n = \bar{V}_i/\bar{L}\bar{C}$ is the nominal control gain, and $V_o(s)$, $U(s)$ and $\Xi_1(s)$ are the Laplace transforms of the output voltage, control signal, and total disturbance, respectively.

Table 7
Nominal parameters of the plant.

Parameter	Symbol	Value
Input voltage	$\bar{V}_i$	10 V
Output voltage	$\bar{V}_o$	2 V
Capacitance	$\bar{C}$	396 μF
Inductance	$\bar{L}$	4.8 μH
Load resistance	$\bar{R}$	7.5 Ω

5.2. Experimental setup

Fig. 14 presents the experimental platform adapted to validate the main contributions of this work. The experimental setup includes: a synchronous buck converter, a controllable active load, a programmable DC power supply (HM305), and the LAUNCHXL-F28377S controller card. With respect to digital implementation, the following features were selected: embedded PWM signals at 200 kHz with dead time (dt) of 20 ns, 12-bits ADC, and sampling period (T_s) of 20 μs. To measure the output voltage, a resistive voltage divider and a first order low pass filter were used. The nominal parameters of the converter are summarized in Table 7.

To generate disturbances, two considerations were taken into account. First, the nominal load $\bar{R}$ is permanently connected to the converter output. Then, to get aggressive current disturbances, an active load $R_d = 2\ \Omega$ is switched to the converter output at fixed frequency by means of Mosfet Q3. Second, to produce uncertainty in control gain, the real input voltage is deviated from its nominal value by an amount denoted by Δ_κ.

5.3. Equivalence tests

To validate the equivalence between GPIO and DOB, a FOGPIO for $n = 2$ and $m = 2$ is proposed as

$$\frac{d}{dt}\hat{v}_o(t) = \dot{\hat{v}}_o(t) + l_3 \left(v_o(t) - \hat{v}_o(t)\right), \tag{59}$$

$$\frac{d}{dt}\dot{\hat{v}}_o(t) = \hat{\xi}(t) + \kappa_n u(t) + l_2 \left(v_o(t) - \hat{v}_o(t)\right), \tag{60}$$

$$\frac{d}{dt}\hat{\xi}(t) = \dot{\hat{\xi}}(t) + l_1 \left(v_o(t) - \hat{v}_o(t)\right), \tag{61}$$

$$\frac{d}{dt}\dot{\hat{\xi}}(t) = l_0 \left(v_o(t) - \hat{v}_o(t)\right), \tag{62}$$

where $L = [l_3 \quad l_2 \quad l_1 \quad l_0]^\top$ is the FOGPIO gain vector.

For the sake of simplicity, all observers are tuned using binomial polynomials, and assuming a bandwidth $\omega_o = 1 \times 10^4$ rad/s. This value was experimentally tuned close to the maximum that could be obtained with the sampling time of 20 μs without observing any unwanted effect.

The characteristic polynomial of the FOGPIO equals to

$$p_{f2} = (s + \omega_o)^4 = s^4 + l_3 s^3 + l_2 s^2 + l_1 s + l_0, \tag{63}$$

where $l_3 = 4 \times 10^4$, $l_2 = 6 \times 10^8$, $l_1 = 4 \times 10^{12}$, and $l_0 = 1 \times 10^{16}$. Therefore, the equivalent Q-filter is

$$Q_{f2} = \frac{l_1 s + l_0}{s^4 + l_3 s^3 + l_2 s^2 + l_1 s + l_0}. \tag{64}$$

Similarly, to estimate the auxiliary vector $\boldsymbol{z}(t) = [z_1 \quad z_2 \quad z_3]^\top$, the ROGPIO for $m = 2$ is designed as

$$\frac{d}{dt}\hat{z}_1(t) = -\lambda_2 \hat{z}_1(t) + \hat{z}_2(t) + \kappa_n u(t) + \left(-\lambda_2^2 + \lambda_1\right) v_o(t), \tag{65}$$

$$\frac{d}{dt}\hat{z}_2(t) = -\lambda_1 \hat{z}_1(t) + \hat{z}_3(t) + \left(-\lambda_1 \lambda_2 + \lambda_0\right) v_o(t), \tag{66}$$

$$\frac{d}{dt}\hat{z}_3(t) = -\lambda_0 \hat{z}_1(t) + \left(-\lambda_0 \lambda_2\right) v_o(t), \tag{67}$$

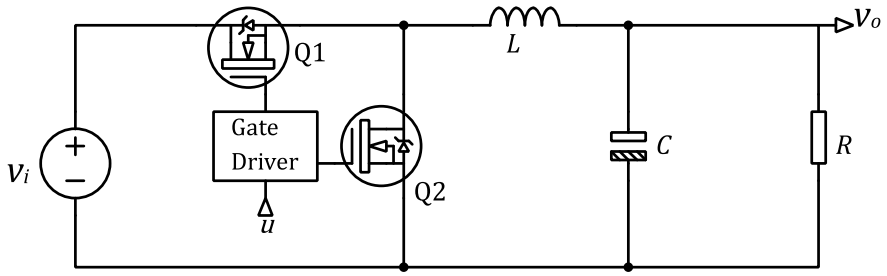

Fig. 13. Circuit diagram of a synchronous buck converter.

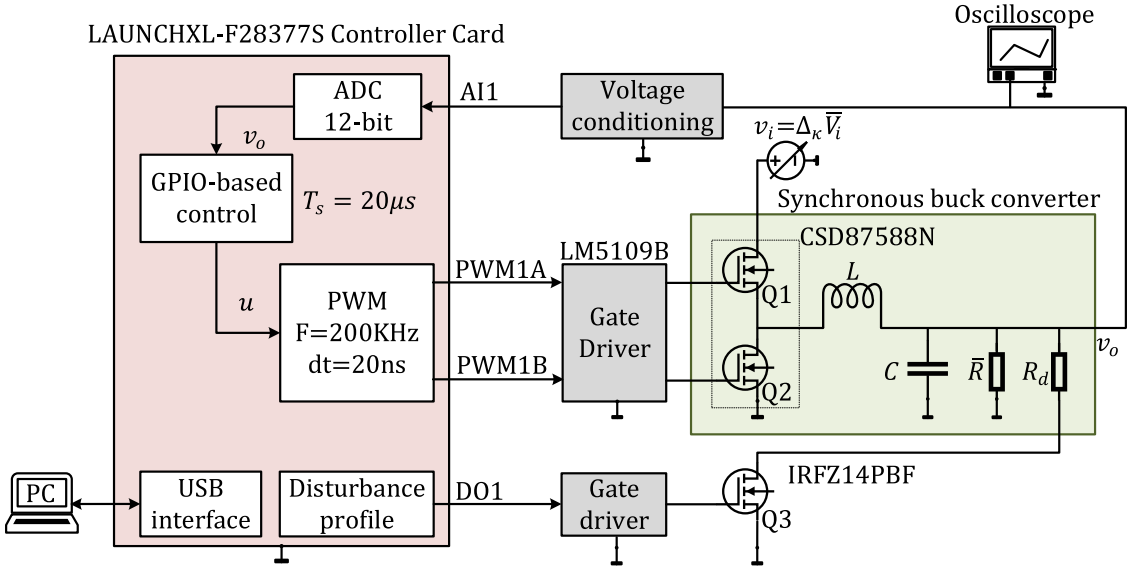

Fig. 14. Experimental setup.

where $L_z = [\lambda_2 \quad \lambda_1 \quad \lambda_0]^\top$ is the observer gain vector, and the real variables are obtained as follows: $\hat{v}_o(t) = \hat{z}_1(t) + \lambda_2 v_o(t)$, $\hat{\xi}(t) = \hat{z}_2(t) + \lambda_1 v_o(t)$, and $\dot{\hat{\xi}}(t) = \hat{z}_3(t) + \lambda_0 v_o(t)$.

The characteristic polynomial of the ROGPIO is

$$p_{r2} = (s + \omega_o)^3 = s^3 + \lambda_2 s^2 + \lambda_1 s + \lambda_0, \tag{68}$$

where $\lambda_2 = 3 \times 10^4$, $\lambda_1 = 3 \times 10^8$, and $\lambda_0 = 1 \times 10^{12}$. As a result, the corresponding Q-filter is

$$Q_{r2} = \frac{\lambda_1 s + \lambda_0}{s^3 + \lambda_2 s^2 + \lambda_1 s + \lambda_0}. \tag{69}$$

The frequency-domain disturbance observer for system (58) is designed as follows:

$$\hat{\Xi}_1(s) = Q(s)\left(s^2/\kappa_n\right) V_o(s) - Q(s)U(s), \tag{70}$$

where $U(s) = U_n(s) - \hat{\Xi}_1(s)$, and $Q(s)$ takes the form of (64) and (69).

Considering that the frequency-domain DOB provides no the estimate of the system states, the following outer loop controller is proposed:

$$U_n(s) = \frac{0.01217s + 243.3}{s + 36000} V_o(s) - \frac{0.07299s + 243.3}{s + 36000} V_o^*(s), \tag{71}$$

where $V_o^*(s)$ is the Laplace transform of the reference signal $(v_o^*(t))$ defined as:

$$v_o^*(t) = 1.5 + 0.5 \sin(20\pi t + 3\pi/2). \tag{72}$$

Figs. 16 and 15 show the equivalence tests for FOGPIO and ROGPIO, respectively. Here, the output voltage $v_o(t)$, the tracking error $v_o(t) - v_o^*(t)$, the control signal $u(t)$, and the estimate of the equivalent input disturbance $\hat{\xi}_1(t)$, are presented for GPIO in comparison with the corresponding DOB implementation. It is worth noting that the active load R_d was toggled at 25 Hz generating sudden periodic disturbances. Besides, the input voltage was reduced by 20% from its nominal value, thus causing uncertainty on the control gain. Results reveal that control schemes produce very similar trajectories for $v_o(t)$. This behavior indicates that, in each case, the inner loop yields the same results, i.e., they are equivalent. Likewise, both the estimate of the disturbance and the control action are similar (overlap) in the two approaches, which also demonstrates the equivalence. There are some small differences in measures, which can be attributed to noise and discretization issues.

5.4. Robustness tests

Table 4 provides the balanced range of the uncertain control gain of ROGPIO for a second-order system. For instance, if the number of extended states equals 2, then, $\Delta_\kappa = \kappa/\kappa_n \in (0.333, 3)$. To verify that this range is reliable, some robustness tests are presented below.

Since $\kappa(t) = v_i(t)/LC$, then, the system response for three different input voltages is analyzed: (1) $v_i(t) = 0.34\bar{V}_i$ (minimum), (2) $v_i(t) = \bar{V}_i$ (nominal), and (3) $v_i(t) = 3\bar{V}_i$ (maximum). The outer loop controller has the general structure presented in Eqs. (45) and (46), whose characteristic polynomial is $p_y(s) = (s+3\times10^3)^2$. Consequently, the nominal control law is defined as

$$u_n(t) = \ddot{v}_o^*(t) - k_0\left(v_o(t) - v_o^*(t)\right) - k_1\left(\dot{\hat{v}}_o(t) - \dot{v}_o^*(t)\right), \tag{73}$$

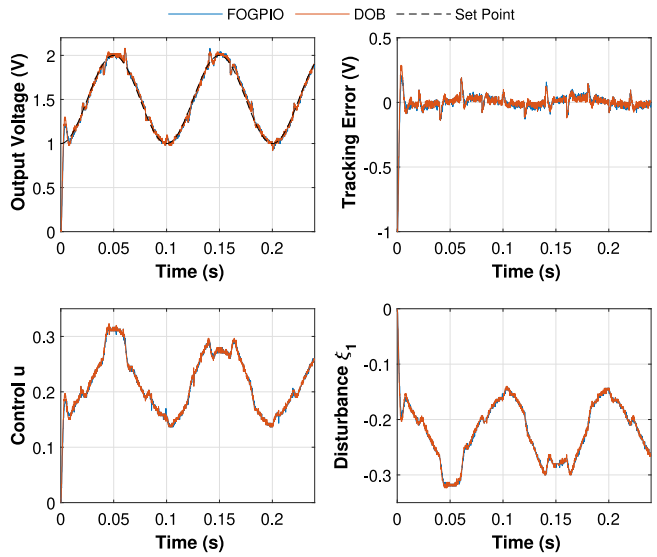

Fig. 15. Experimental validation of the equivalence between FOGPIO and DOB.

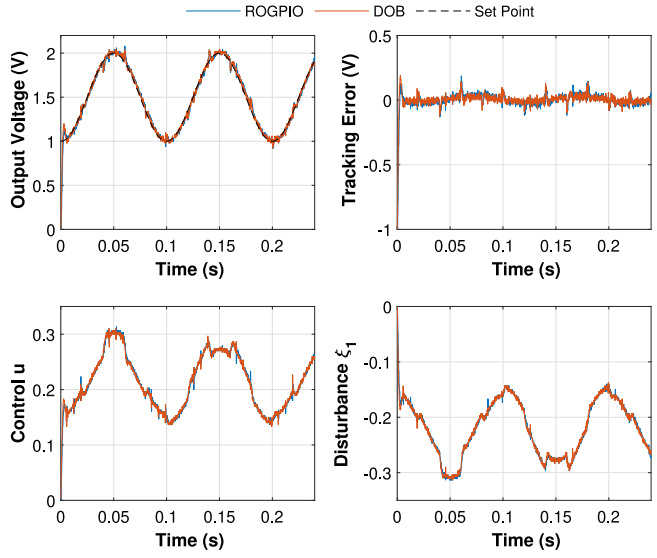

Fig. 16. Experimental validation of the equivalence between ROGPIO and DOB.

where $k_0 = 9\times10^6$, $k_1 = 6\times10^3$, $\dot{\hat{v}}_o(t)$ is provided by the designed ROGPIO, and the reference is (72).

To facilitate the visualization of the effect of the load disturbance, the resistance varies as follows:

$$R = \begin{cases} \bar{R}, & \text{for} \quad t \in [0, 0.1)\ \text{s}, \\ 0.21\bar{R}, & \text{for} \quad t \in [0.1, 0.2)\ \text{s}, \\ \bar{R}, & \text{for} \quad t \in [0.2, 0.24)\ \text{s}. \end{cases} \tag{74}$$

Fig. 17 presents the robustness validation of the ROGPIO against uncertainty on control gain. The output voltage, the tracking error, the control signal, and the estimated disturbance are used to compare the system performance assuming changes in $\kappa(t)$. Results show that stability is guaranteed within the full range of Δ_κ. When the nominal load is present, the tracking error remains close to its steady-state nominal value, regardless of whether $\kappa(t)$ increases or decreases. For sudden changes in the load ($t = 0.1$ s and $t = 0.2$ s), the control action is also effective. However, for large $\kappa(t)$ (in blue) the signal-to-noise ratio (in control) worsens, thus making the current ripple more

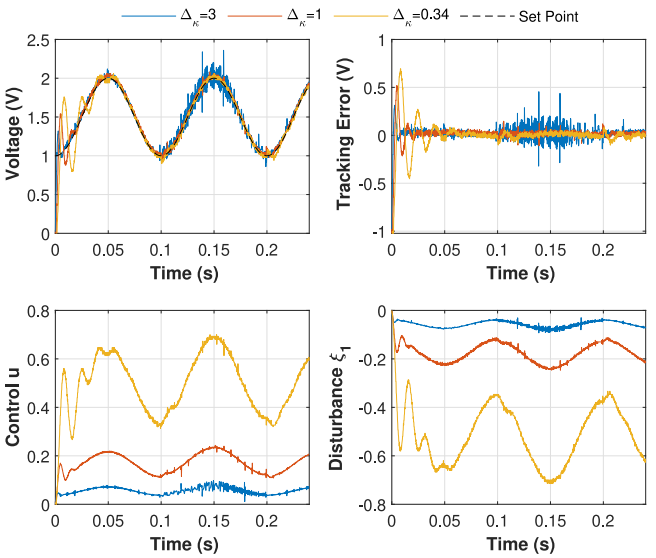

Fig. 17. Robustness validation of ROGPIO against uncertainty on control gain. No filters are applied. (For interpretation of the references to color in this figure legend, the reader is referred to the web version of this article.)

evident for hard loads ($0.1\ \text{s} \leq t \leq 0.2\ \text{s}$), and degrading the performance.

5.5. Comparison between ROGPIO and FOGPIO

In this subsection an experimental comparison between full-order and reduced-order GPIO is presented. The tests use the set point (72), the time-domain reference model (57), and the nominal control law (73). In addition, the alternative control law (52) that uses the estimate of the output ($\hat{v}_o(t)$) instead of its measurement ($v_o(t)$), is included. For ease of visualization, only the nominal load is considered.

The response curves of the output voltage and the tracking error for one and two extended states are depicted in Fig. 18. Results illustrate that the tracking error of ROGPIO is the smallest in each case, which matches with the values in Fig. 12. The tracking error in the FOGPIO slightly increases by using the estimate of the output. Since the outer loop controller is the same in all tests, the tracking error depends largely on the estimation error (inner loop). Therefore, by increasing the number of extended states, the closed-loop performance improves strongly.

5.6. Performance tests

A simple way to validate the influence of the number of extended states on the performance of GPIO is to build a practical Bode plot of the inner loop. This involves depicting the frequency-response of the transfer function $V_o(s)/U_n(s)$, and comparing it with the desired linear reference model.

As mentioned above, the possibility of choosing a nominal model is a distinctive feature of disturbance rejection based control. In this regard, some desirable characteristics, such as the nominal control gain, no amplification, and a practical dc-gain, are taken into account in this test. Therefore, consider the following reference model to build the Bode plot:

$$P_n(s) = \frac{\bar{V}_i/\bar{L}\bar{C}}{(s + 1/\bar{L}\bar{C})^2}. \tag{75}$$

Note that (75) has the same order and nominal control gain as the real plant, but it has no the integrator chain form.

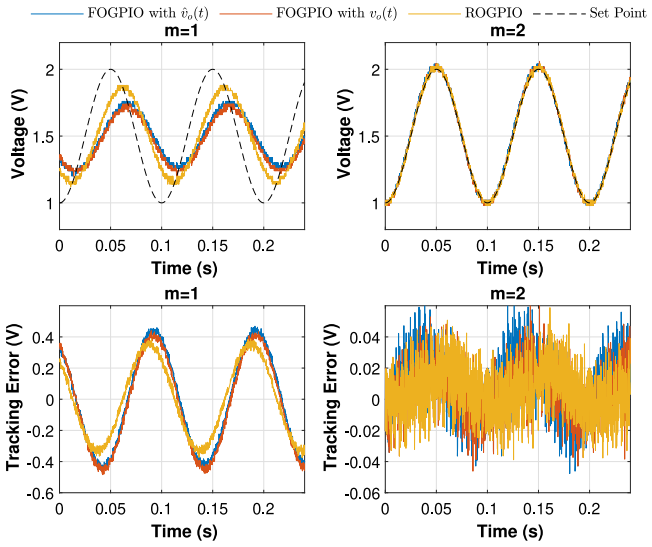

Fig. 18. Experimental comparison between FOGPIO and ROGPIO. No filters are applied.

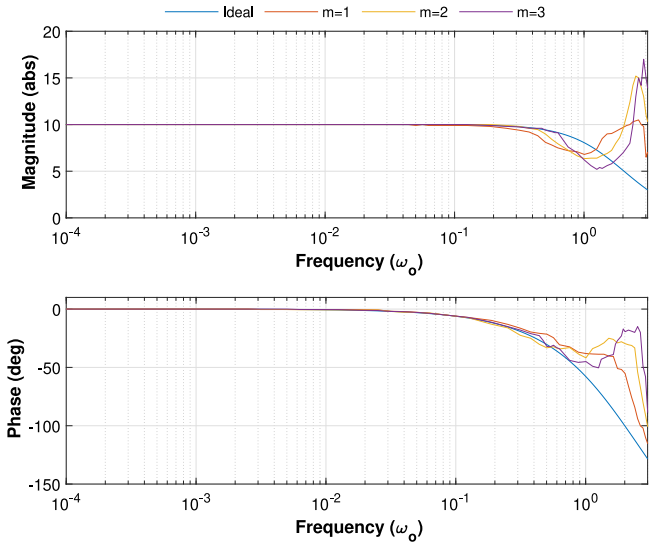

Fig. 19. Experimental bode plot of ROGPIO ($V_o(s)/U_n(s)$) for $m \in [1, 3]$. (For interpretation of the references to color in this figure legend, the reader is referred to the web version of this article.)

During the experiment, the active load R_d is switched at 100 Hz, the input voltage corresponds to its nominal value, and the nominal control path satisfies the following equation:

$$u_n(t) = 0.2 + 0.1 \sin(\omega_u t), \tag{76}$$

where $\omega_u \in [0, 3 \times 10^4]$ rad/s.

Fig. 19 depicts the experimental Bode plot of the ROGPIO for $m \in [1, 3]$. The characteristic polynomial is $p_r = (s + \omega_o)^{m+1}$, where $\omega_o = 1 \times 10^4$ rad/s. Results show how the linearization process is carried out in comparison with the ideal reference model (in blue). As expected, the effective bandwidth ω_S increases with m and it is close to that presented in Table 3. Finally, it is possible to establish that for frequencies less than ω_S, the disturbance rejection is reliable. However, noise amplification can limit the practical use of observers with a high number of extended states.

6. Conclusions

This paper showed that generalized proportional integral observer (GPIO) can be equivalent to disturbance observer (DOB). This premise was demonstrated with a frequency-domain approach, which revealed the specific structure of the Q-filter of DOB that meets the equivalence. In this way, the procedure was applied to ADRC schemes with different observers (FOGPIO, ROGPIO, ESO, and RESO), whose reference models have the integrator chain form. Based on this equivalence, the robustness and performance of GPIO were analyzed. As a result, some guidelines for the practical implementation of GPIO were obtained regarding the influence of the system order, the number of extended states, the uncertain control gain, and the tuning method

The equivalence also provided a framework for evaluating the considered disturbance estimation methods, in terms of their design principles and relations. In this context, the study articulated several practical control requirements, such as robustness margins, accuracy/performance, and noise sensitivity, thus addressing a pressing need in the field of ADRC. The equivalence was successfully validated on the voltage control of a synchronous buck converter affected by disturbances in the input voltage and the load. Experimental tests confirmed that the proposed analyses can be used as reliable insights for GPIO-based control.

Declaration of competing interest

The authors declare that they have no known competing financial interests or personal relationships that could have appeared to influence the work reported in this paper.

Acknowledgments

Harvey David Rojas want to thank MinCiencias - Colombia for his Ph.D. scholarship provided by *"Programa de Becas de Excelencia Doctoral del Bicentenario - Corte 1 (2019)"*

References

[1] Sariyildiz E, Oboe R, Ohnishi K. Disturbance observer-based robust control and its applications: 35th anniversary overview. IEEE Trans Ind Electron 2020;67(3):2042–53. http://dx.doi.org/10.1109/TIE.2019.2903752, arXiv:1902.09032.

[2] Chen S, Bai W, Hu Y, Huang Y, Gao Z. On the conceptualization of total disturbance and its profound implications. Sci China Inf Sci 2020;63(2):1–3. http://dx.doi.org/10.1007/s11432-018-9644-3.

[3] Chen WH, Yang J, Guo L, Li S. Disturbance-observer-based control and related methods - an overview. IEEE Trans Ind Electron 2016;63(2):1083–95. http://dx.doi.org/10.1109/TIE.2015.2478397.

[4] Huang Y, Xue W. Active disturbance rejection control: Methodology and theoretical analysis. ISA Trans 2014;53(4):963–76. http://dx.doi.org/10.1016/j.isatra.2014.03.003.

[5] Rojas-Cubides H, Cortés-Romero J, Coral-Enriquez H, Rojas-Cubides H. Sliding mode control assisted by GPI observers for tracking tasks of a nonlinear multivariable twin-rotor aerodynamical system. Control Eng Pract 2019;88:1–15. http://dx.doi.org/10.1016/j.conengprac.2019.04.002.

[6] Sariyildiz E, Ohnishi K. A guide to design disturbance observer. J Dyn Syst Meas Control 2019;1:1–42, arXiv:1912.06331.

[7] Li S, Yang J, Chen WH, Chen X. Disturbance observer-based control methods and applications. CRC Press. Taylor & Francis Group; 2014, p. 314. http://dx.doi.org/10.1201/b16570.

[8] Gao Z. Active disturbance rejection control: From an enduring idea to an emerging technology. In: 2015 10th international workshop on robot motion and control, RoMoCo 2015. Institute of Electrical and Electronics Engineers Inc.; 2015, p. 269–82. http://dx.doi.org/10.1109/RoMoCo.2015.7219747.

[9] Zheng Q, Gao Z. Active disturbance rejection control: between the formulation in time and the understanding in frequency. Control Theory Technol 2016;14(3):250–9. http://dx.doi.org/10.1007/s11768-016-6059-9.

[10] Sira-Ramírez H. From flatness, GPI observers, GPI control and flat filters to observer-based ADRC. Control Theory Technol 2018;16(4):249–60. http://dx.doi.org/10.1007/s11768-018-8134-x.

[11] Bickel R, Tomizuka M. Passivity-based versus disturbance observer based robot control: Equivalence and stability. J Dyn Syst Meas Control Trans ASME 1999;121(1):41–7. http://dx.doi.org/10.1115/1.2802440.

[12] Schrijver E, Van Dijk J. Disturbance observers for rigid mechanical systems: Equivalence, stability, and design. J Dyn Syst Meas Control Trans ASME 2002;124(4):539–48. http://dx.doi.org/10.1115/1.1513570.

[13] Kim BK, Choi HT, Chung WK, Suh IH. Analysis and design of robust motion controllers in the unified framework. J Dyn Syst Meas Control Trans ASME 2002;124(2):313–21. http://dx.doi.org/10.1115/1.1468995.

[14] Garrido R, Luna JL. On the equivalence between PD+DOB and PID controllers applied to servo drives. IFAC-PapersOnLine 2018;51(4):95–100. http://dx.doi.org/10.1016/j.ifacol.2018.06.044.

[15] Rahman FMM, Pirsto V, Kukkola J, Hinkkanen M, Perez-Estevez D, Doval-Gandoy J. Equivalence of the integrator-based and disturbance-observer-based state-space current controllers for grid converters. IEEE Trans Ind Electron 2021;68(6):4966–76. http://dx.doi.org/10.1109/TIE.2020.2988194.

[16] Jung S, Lee JW. Similarity analysis between a nonmodel-based disturbance observer and a time-delayed controller for robot manipulators in cartesian space. IEEE Access 2021;9:122299–307. http://dx.doi.org/10.1109/ACCESS.2021.3109568.

[17] Su J, Wang L, Yun JN. A design of disturbance observer in standard h∞ control framework. Internat J Robust Nonlinear Control 2015;25(16):2894–910. http://dx.doi.org/10.1002/rnc.3235.

[18] Seo HT, Kim S, Kim KS. An H∞ design of disturbance observer for a class of linear time-invariant single-input/single-output systems. Int J Control Autom Syst 2020;18(7):1662–70. http://dx.doi.org/10.1007/s12555-019-0045-1.

[19] Sira-Ramirez H, Zurita-Bustamante EW, Huang C. Equivalence among flat filters, dirty derivative-based PID controllers, ADRC, and integral reconstructor-based sliding mode control. IEEE Trans Control Syst Technol 2019;1–15. http://dx.doi.org/10.1109/tcst.2019.2919822.

[20] Sira-Ramírez H, Zurita-Bustamante EW. On the equivalence between ADRC and flat filter based controllers: A frequency domain approach. Control Eng Pract 2021;107:104656. http://dx.doi.org/10.1016/j.conengprac.2020.104656.

[21] Jin H, Song J, Lan W, Gao Z. On the characteristics of ADRC: a PID interpretation. Sci China Inf Sci 2020;63(10):1–3. http://dx.doi.org/10.1007/s11432-018-9647-6.

[22] Ahmad S, Ali A. Unified disturbance-estimation-based control and equivalence with IMC and PID: Case study on a DC-DC boost converter. IEEE Trans Ind Electron 2021;68(6):5122–32. http://dx.doi.org/10.1109/TIE.2020.2987269.

[23] Lin P, Sun X-M, Fei Z. A generalized interpretation of three types of disturbance-based controllers for perturbed integral systems in frequency domain. IEEE Trans Circuits Syst II: Express Briefs 2021;68(4):1328–32. http://dx.doi.org/10.1109/TCSII.2020.3026687.

[24] Zhou R, Fu C, Tan W. Implementation of linear controllers via active disturbance rejection control structure. IEEE Trans Ind Electron 2021;68(7):6217–26. http://dx.doi.org/10.1109/TIE.2020.2992951.

[25] Madoński R, Herman P. Survey on methods of increasing the efficiency of extended state disturbance observers. ISA Trans 2015;56:18–27. http://dx.doi.org/10.1016/j.isatra.2014.11.008.

[26] Ahmad S, Ali A. Active disturbance rejection control of DC–DC boost converter: A review with modifications for improved performance. IET Power Electron 2019;12(8):2095–107. http://dx.doi.org/10.1049/iet-pel.2018.5767.

[27] Ahi B, Haeri M. Linear active disturbance rejection control from the practical aspects. IEEE/ASME Trans Mechatronics 2018;23(6):2909–19. http://dx.doi.org/10.1109/TMECH.2018.2871880.

[28] Xue W, Huang Y. Performance analysis of active disturbance rejection tracking control for a class of uncertain LTI systems. ISA Trans 2015;58(2014):133–54. http://dx.doi.org/10.1016/j.isatra.2015.05.001.

[29] Tian G, Gao Z. Frequency response analysis of active disturbance rejection based control system. In: Proceedings of the IEEE international conference on control applications. 2007, p. 1595–9. http://dx.doi.org/10.1109/CCA.2007.4389465.

[30] Huang C, Zheng Q. Frequency response analysis of linear active disturbance rejection control. Sens Transducers 2013;157(10):346–54.

[31] Xue W, Huang Y. On frequency-domain analysis of ADRC for uncertain system. In: Proceedings of the American control conference. 2013, p. 6637–42. http://dx.doi.org/10.1109/acc.2013.6580881.

[32] Zhong S, Huang Y. Comparison of the phase margins of different ADRC designs. In: Chinese control conference, CCC, Vol. 2019-July. IEEE Computer Society; 2019, p. 1280–5. http://dx.doi.org/10.23919/ChiCC.2019.8865297.

[33] Jin H, Liu L, Lan W, Zeng J. On stability and robustness of linear active disturbance rejection control: A small gain theorem approach. In: Chinese control conference, CCC. IEEE Computer Society; 2017, p. 3242–7. http://dx.doi.org/10.23919/ChiCC.2017.8027857.

[34] Wu D, Chen K. Frequency-domain analysis of nonlinear active disturbance rejection control via the describing function method. IEEE Trans Ind Electron 2013;60(9):3906–14. http://dx.doi.org/10.1109/TIE.2012.2203777.

[35] Li J, Qi X, Xia Y, Pu F, Chang K. Frequency domain stability analysis of nonlinear active disturbance rejection control system. ISA Trans 2015;56:188–95. http://dx.doi.org/10.1016/j.isatra.2014.11.009.

[36] Li J, Xia Y, Qi X, Zhao P. Robust absolute stability analysis for interval nonlinear active disturbance rejection based control system. ISA Trans 2017;69:122–30. http://dx.doi.org/10.1016/j.isatra.2017.04.017.

[37] Qi X, Li J, Xia Y, Gao Z. On the robust stability of active disturbance rejection control for SISO systems. Circuits Systems Signal Process 2017;36(1):65–81. http://dx.doi.org/10.1007/s00034-016-0302-y.

[38] Li S, Yang J, Chen WH, Chen X. Generalized extended state observer based control for systems with mismatched uncertainties. IEEE Trans Ind Electron 2012;59(12):4792–802. http://dx.doi.org/10.1109/TIE.2011.2182011.

[39] Gao Z. Scaling and bandwidth-parameterization based controller tuning. In: Proceedings of the American control conference, Vol. 6. 2003, p. 4989–96. http://dx.doi.org/10.1109/acc.2003.1242516.

[40] Skogestad S, Postlethwaite I. Multivariable feedback control. Analysis and design. 2nd ed.. Wiley; 2005, p. 590.

[41] Seiler P, Packard A, Gahinet P. An introduction to disk margins [lecture notes]. IEEE Control Syst Mag 2020;40(5):78–95. http://dx.doi.org/10.1109/MCS.2020.3005277.

[42] Graham D, Lathrop RC. The synthesis of "optimum" transient response: Criteria and standard forms. Trans Amer Inst Electr Eng II 1953;72(5):273–88. http://dx.doi.org/10.1109/tai.1953.6371346.

[43] Marshax AH, Johnson DE, Johnson JR. A bessel rational filter. IEEE Trans Circuits Syst 1974;21(6):797–9. http://dx.doi.org/10.1109/TCS.1974.1083932.

[44] Yang H, Zhang Y, Liang J, Liu J, Zhang N, Walker PD. Robust deadbeat predictive power control with a discrete-time disturbance observer for PWM rectifiers under unbalanced grid conditions. IEEE Trans Power Electron 2018;34(1):287–300. http://dx.doi.org/10.1109/TPEL.2018.2816742.

[45] Erickson RW, Maksimović D. Fundamentals of power electronics. 2nd ed,. Boston, MA: Springer; 2001, p. 331–75. http://dx.doi.org/10.1007/b100747.

[46] Wang J, Li S, Yang J, Wu B, Li Q. Extended state observer-based sliding mode control for PWM-based DC-DC buck power converter systems with mismatched disturbances. IET Control Theory Appl 2015;9(4):579–86. http://dx.doi.org/10.1049/iet-cta.2014.0220.

[47] Rojas-Cubides H, Cortés-Romero J, Arcos-Legarda J. Data-driven disturbance observer-based control: an active disturbance rejection approach. Control Theory Technol 2021. http://dx.doi.org/10.1007/s11768-021-00039-x.

[48] Figueres E, Garcerá G, Benavent JM, Pascual M, Martínez JA. Adaptive two-loop voltage-mode control of DC-DC switching converters. IEEE Trans Ind Electron 2006;53(1):239–53. http://dx.doi.org/10.1109/TIE.2005.862254.